Long-Time-Series Global Land Surface Satellite Leaf Area Index Product Derived From MODIS and AVHRR Surface Reflectance

Zhiqiang Xiao, Shunlin Liang, *Fellow, IEEE*, Jindi Wang, Yang Xiang, Xiang Zhao, and Jinling Song

***Abstract*—Leaf area index (LAI) is an important vegetation biophysical variable and has been widely used for crop growth monitoring and yield estimation, land-surface process simulation, and global change studies. Several LAI products currently exist, but most have limited temporal coverage. A long-term high-quality global LAI product is required for greatly expanded application of LAI data. In this paper, a method previously proposed was improved to generate a long time series of Global LAnd Surface Satellite (GLASS) LAI product from Advanced Very High Resolution Radiometer (AVHRR) and Moderate Resolution Imaging Spectroradiometer (MODIS) reflectance data. The GLASS LAI product has a temporal resolution of eight days and spans from 1981 to 2014. During 1981–1999, the LAI product was generated from AVHRR reflectance data and was provided in a geographic latitude/longitude projection at a spatial resolution of 0.05°. During 2000–2014, the LAI product was derived from MODIS surface-reflectance data and was provided in a sinusoidal projection at a spatial resolution of 1 km. The GLASS LAI values derived from MODIS and AVHRR reflectance data form a consistent data set at a spatial resolution of 0.05°. Comparison of the GLASS LAI product with the MODIS LAI product (MOD15) and the first version of the Geoland2 (GEOV1) LAI product indicates that the global consistency of these LAI products is generally good. However, relatively large discrepancies among these LAI products were observed in tropical forest regions, where the GEOV1 LAI values were clearly lower than the GLASS and MOD15 LAI values, particularly in January. A quantitative comparison of temporal profiles shows that the temporal smoothness of the GLASS LAI product is superior to that of the GEOV1 and MODIS LAI products. Direct validation with the mean values of high-resolution LAI maps demonstrates that the GLASS LAI values were closer to the mean values of the high-resolution LAI maps (RMSE $= 0.7848$ and $R^2 = 0.8095$) than the GEOV1 LAI values (RMSE $= 0.9084$ and $R^2 = 0.7939$) and the MOD15 LAI values (RMSE $= 1.1173$ and $R^2 = 0.6705$).**

***Index Terms*—Advanced Very High Resolution Radiometer (AVHRR), Global LAnd Surface Satellite (GLASS) products, leaf area index (LAI), Moderate Resolution Imaging Spectroradiometer (MODIS), neural networks, time series, validation.**

Manuscript received March 20, 2015; revised November 18, 2015, February 15, 2016, and March 28, 2016; accepted April 25, 2016. This work was supported in part by the Chinese 863 Program under Grant 2013AA121201, by the Chinese 973 Program under Grant 2013CB733403, and by the National Natural Science Foundation of China under Grant 41171264 and Grant 41331173.

This paper has supplementary downloadable material available at http://ieeexplore.ieee.org, provided by the authors.

Z. Xiao, J. Wang, Y. Xiang, X. Zhao, and J. Song are with the State Key Laboratory of Remote Sensing Science, School of Geography, Beijing Normal University, Beijing 100875, China (e-mail: zhqxiao@bnu.edu.cn).

S. Liang is with the Department of Geography, University of Maryland, College Park, MD 20742 USA (e-mail: sliang@geog.umd.edu).

Color versions of one or more of the figures in this paper are available online at http://ieeexplore.ieee.org.

Digital Object Identifier 10.1109/TGRS.2016.2560522

I. Introduction

LEAF area index (LAI) is defined as one-half the total green leaf area per unit of horizontal ground surface area and is called true LAI [1]. The true LAI multiplied by the clumping index, which quantifies the level of foliage grouping within distinct canopy structures relative to a random distribution [2], is called effective LAI. LAI is an important vegetation biophysical variable and has been widely used for crop growth monitoring and yield estimation, land-surface process simulation, and many other global change studies. The estimation of LAI from remote sensing data is the only feasible way to generate LAI products at regional and global scales.

Many methods have been developed to retrieve LAI from satellite remote sensing data [3], [4]. In general, two methods have been used: empirical and physical. The empirical methods are based on statistical relationships between LAI and spectral vegetation indexes, which are calibrated for distinct vegetation types using field measurements of LAI and reflectance data recorded by a remote sensor or simulations with canopy radiation models [5]. The physical methods are based on the inversion of canopy radiative transfer models through iterative minimization of a cost function [6], [7], the lookup table (LUT) method [8], or various machine learning methods [9]. Inversion techniques based on the iterative minimization of a cost function require hundreds of runs of the canopy radiative transfer model for each pixel and are therefore computationally exceedingly demanding. For practical applications, the LUT and artificial neural network methods are two popular inversion techniques that are based on a previously computed reflectance database.

Currently, multiple global LAI products have been generated from various types of satellite remote sensing data [10], [11]. These products are retrieved using various methods and possess different spatial and temporal resolutions. Some major global LAI products are listed in Table I. A comparison of these LAI products indicates that the global consistency of the first version of the Geoland2 (GEOV1) LAI product and the Moderate Resolution Imaging Spectroradiometer (MODIS) LAI product (MOD15) is good in most situations [12] and that the CYCLOPES, MOD15, and GLOBCARBON LAI values agree better over croplands and grasslands than over forests [13]. Qualitative analysis of temporal profiles shows that the CYCLOPES, MOD15, GLOBCARBON, and GEOV1 LAI products display consistent seasonal variations over most vegetation types [12], [13]. Direct validation shows that the MOD15 and CYCLOPES LAI products are the most accurate over grass

TABLE I
CHARACTERISTICS OF MAJOR GLOBAL LAI PRODUCTS

LAI product	Satellite/Sensor	Spatial resolution	Temporal resolution/span	Algorithm	References
GLOBCARBON	SPOT/VEGETATION ENVISAT/AATSR (ENVISAT/ATSR-2 (1998-2002))	1/11.2° (~ 10 km)	1 month 1998–2007	Semi-empirical relationship (SR, RSR VI, BRDF correction, and temporal filter)	Deng et al. [21]
CYCLOPES	SPOT/VEGETATION	1/112° (~ 1 km)	10 days 1999–2007	Radiative-transfer inversion by neural networks	Baret et al. [9]
MOD15	TERRA-AQUA/MODIS	1 km	8 days 2000–	Radiative-transfer inversion by LUT	Knyazikhin et al. [22]
GIMMS3g	AVHRR	1/12° (~ 8 km)	15 days 1981–2011	Feedforward neural networks	Zhu et al. [23]
GEOV1	SPOT/VEGETATION	1/112° (~ 1 km)	10 days 1998–	Backpropagation neural networks capitalizing on existing LAI products	Baret et al. [24]
GLASS	MODIS, AVHRR	0.05° (~ 5km) 1 km	8 days 1981–	General regression neural networks	This paper

and croplands, but that large uncertainties are observed for these products over evergreen broadleaf forests [13]–[15]. Considerable progress has been made, and different products have been extensively used in various applications [4]. However, many issues remain in generating these LAI products from satellite data, and these have a direct impact on quality and accuracy.

First, these LAI products are routinely generated from remote sensing data acquired only at a specific time. Because limited information is used for the inversion process, these products are not spatially and temporally continuous. They are frequently missing in winter over northern latitudes and over the Equatorial belt [13] and exhibit many time-series fluctuations, particularly during vegetation growing seasons [16]. These LAI products are also inaccurate for some vegetation types such as evergreen broadleaf forest [13], [17], [18]. Low accuracy and poor quality in many cases among existing LAI products certainly call for improvements and new products. It is easy to improve the quality (e.g., smoothing, missing data) of existing products, but accuracy cannot be improved without generating a new product. One potential solution to these problems is to retrieve LAI using multitemporal signatures. Xiao *et al.* [7] developed a temporally integrated inversion method to estimate LAI from MODIS reflectance time-series data. The parameters of a double-logistic LAI temporal-profile model coupled with a radiative-transfer model were estimated in such a way that the surface reflectances simulated with the radiative-transfer model optimally matched the MODIS reflectance time-series data from the growing seasons. Smoothed LAI profiles with improved accuracy were then reconstructed using the LAI temporal-profile model parameters. Liu *et al.* [19] developed a similar method to retrieve LAI by combining the MODIS albedo product with a dynamic leaf model. The results showed that the seasonal cycle of the directly retrieved leaf areas was smooth and consistent with both observations and current understanding of the processes controlling leaf area dynamics [19]. These methods assumed that all observations were available in advance and were therefore suitable for historical data analysis. To monitor rapid land-surface changes, Xiao *et al.* [20] developed a real-time inversion method to estimate LAI using MODIS reflectance time-series data. As new observations arrived, an ensemble Kalman filter was used to update the LAI recursively by combining predictions from dynamic models and MODIS reflectance data. In the absence of new observations, the biophysical variables could be propagated using the dynamic models. All these studies have demonstrated the ability to retrieve biophysical parameters supplied by the time series of remote sensing observations.

Second, existing LAI products are based mainly on individual satellite data that usually cover the same short periods as the satellite missions. For example, the MOD15 LAI product is based on TERRA/MODIS data, the third-generation Global Inventory Modeling and Mapping Studies (GIMMS3g) LAI product is based on Advanced Very High Resolution Radiometer (AVHRR) data, and the GEOV1 LAI product is based on SPOT/VEGETATION data. Efforts are being made to produce the climate data record from multiple satellite data sets. The climate data record is defined as a time series of measurements of sufficient length, consistency, and continuity to describe climate variability and change [25]. Using neural networks and temporal filtering techniques, Verger *et al.* [26] developed a multisensor fusion approach to improve the spatiotemporal continuity, consistency, and accuracy of current satellite products. The fusion product derived from available VEGETATION and MODIS observations was able to fill in most of the missing LAI values with improved temporal smoothness and better agreement with ground measurements. The multisensor fusion approach may contribute to generating continuous long-term Earth System Data Records from remote sensing data collected from several sensors [26]. However, most global LAI products still involve a short time series [13]. There is a strong need for a robust algorithm to generate a long-term LAI product from multiple satellite data.

To exploit fully the potential of multitemporal remote sensing data, Xiao *et al.* [27] developed a method to estimate LAI from MODIS surface-reflectance time-series data using general regression neural networks (GRNNs). Unlike existing neural network methods that use only remote sensing data acquired at a specific time to retrieve LAI, the preprocessed MODIS reflectance data for a one-year period were input into the GRNNs to estimate the one-year LAI profiles. Extensive validations have demonstrated that this method is able to estimate temporally continuous LAI profiles with much improved

accuracy compared with that of MOD15 and CYCLOPES [27]. Because of the excellent performance of this method in retrieving LAI from MODIS reflectance time-series data, it was extended in this study to retrieve LAI from AVHRR reflectance time-series data. Moreover, a processing strategy was proposed to generate a long time series of temporally continuous Global LAnd Surface Satellite (GLASS) LAI product (1981–2014) from MODIS and AVHRR reflectance time-series data. The consistency of GLASS LAI values derived from AVHRR and MODIS reflectance data was evaluated. This paper also analyzes the discrepancies between the GLASS LAI product and other existing global LAI products, including MOD15 and GEOV1 LAI products. The accuracy of the GLASS LAI product was evaluated against high-resolution LAI maps.

The organization of this paper is as follows. Section II describes the observed satellite data, existing global LAI products, and LAI ground measurements. Section III describes the algorithm that uses GRNNs for LAI retrieval from MODIS and AVHRR reflectance time-series data and the processing strategy to generate a long time series of temporally continuous GLASS LAI product. The method used to evaluate the GLASS LAI product is also described in this section. The results of a consistency analysis between the GLASS LAI values derived from AVHRR and MODIS reflectance data, a comparison between the GLASS LAI product and other existing global LAI products, and a direct validation of the GLASS LAI product against high-resolution LAI maps are presented in Section IV; discussions are presented in Section V, and conclusions are drawn in Section VI.

II. Data and Preprocessing

A. MODIS and AVHRR Surface Reflectance Data

The MODIS surface reflectance product (MOD09A1), in a sinusoidal projection system, was derived from the latest version (Collection 5) and was downloaded from http://reverb.echo.nasa.gov/reverb/. The MOD09A1 product has been produced since 2000 at a 500-m spatial resolution and an eight-day temporal sampling period [28]. The AVHRR reflectance data were from NASA's Land Long-Term Data Record (LTDR) project [29]. The LTDR AVHRR reflectance product, with a spatial resolution of 0.05° and a daily temporal sampling period, uses a geographic latitude/longitude projection. The latest version (Version 3) was used in this study. The LTDR AVHRR reflectance product for 1981–1999 was downloaded from http://ltdr.nascom.nasa.gov/, and the product for 2003–2004 was provided by Dr. Eric Vermote.

Although the quality of the MODIS and LTDR AVHRR reflectance data was greatly improved, some cloudy or partially cloudy pixels remained in the data, and reflectance data were still missing for some days in the series. The MODIS and AVHRR reflectance data were preprocessed to remove cloud contamination and fill any gaps using a new time-series cloud-detection (TSCD) algorithm [30]. The TSCD algorithm is based on the assumptions of relatively stable surface reflectance and of rapid temporal variations in reflectance due to cloud contamination. Cloud-contaminated data were removed using a temporal spatial filter method that integrates temporal, spatial, spectral, and flag information, and missing data were filled in using an optimum interpolation algorithm to obtain continuous and smooth surface reflectance values. The validation results demonstrated that the TSCD algorithm performs very well, particularly when the land surface is stable or slowly changing [25].

In this paper, MODIS and AVHRR reflectance time series in the red and near-infrared spectral bands were used to estimate LAI profiles. The MODIS reflectance data were aggregated to a 1-km resolution using an average method to maintain a spatial resolution consistent with the MOD15 and CYCLOPES LAI products. The maximum-value composite (MVC) approach [31] was used to composite the daily AVHRR surface-reflectance data into eight-day intervals to maintain a temporal resolution consistent with the MODIS surface-reflectance data. The MVC approach selected the AVHRR reflectance data with the highest normalized difference vegetation index (NDVI) over each eight-day time interval.

B. Global LAI Products

This section describes the main characteristics of the MOD15, CYCLOPES, GEOV1, and GLASS LAI products investigated in this study. A summary of these with their main characteristics can be found in Table I.

The MOD15 LAI product (MOD15A2) has been available since 2000 and is provided in a sinusoidal projection at a 1-km spatial resolution and an eight-day time step [8]. The latest version of the MOD15 LAI product is Collection 5 and is used in this study. The MOD15 LAI retrieval algorithm includes a main algorithm and a backup algorithm. The main algorithm is based on LUTs simulated from a 3-D radiative-transfer model for the eight main biome classes according to MODIS land cover and the backup algorithm estimated LAI from biome-specific LAI-NDVI relationships [22]. The MOD15 LAI product provides quality control (QC) information to indicate the quality of LAI values. Among them, SCF_QC are 3 binary bits indicating LAI algorithms. If bit combinations of SCF_QC are 000 or 001, the LAI values are retrieved from the main algorithm. If bit combinations of SCF_QC are 010 or 011, the main algorithm fails due to poor geometry or other problems, and the backup algorithm is used to estimate LAI values [8]. Generally, LAI estimates using the backup algorithm are of lower quality, mainly because of residual clouds and poor atmospheric correction [14].

The CYCLOPES LAI product, with a spatial resolution of 1/112° (about 1 km at the Equator) and a ten-day temporal sampling period, was generated from SPOT/VEGETATION sensor data for 1999–2007 [9]. This product was projected in plate carrée. The algorithm used to estimate CYCLOPES LAI values was based on training backpropagation neural networks with a PROSPECT+SAIL radiative-transfer-model simulation [9]. The GEOV1 LAI product has been available since 1998 from http://www.geoland2.eu/. The product is also provided in a plate carrée projection at 1/112° spatial resolution and a ten-day frequency. The GEOV1 LAI product was derived from SPOT/VEGETATION sensor data using backpropagation neural networks that were trained by fused and scaled "best estimates" of LAI from the MOD15 and CYCLOPES products

and the SPOT/VEGETATION nadir surface reflectance values over the Benchmark Land Multisite Analysis and Intercomparison of Products (BELMANIP) network of sites [24]. The CYCLOPES and GEOV1 LAI products were reprojected onto the sinusoidal projection used in the MOD15 and GLASS LAI products using the General Cartographic Transformation Package map projection library [32] and resampled to a 1-km spatial resolution using the nearest-neighbor resampling method.

The GLASS LAI product has a temporal resolution of eight days and spans from 1981 to 2014. For 1981–1999, the LAI product was generated from LTDR AVHRR reflectance data. It was provided in a geographic latitude/longitude projection at a spatial resolution of 0.05° (about 5 km at the Equator). For 2000–2014, the LAI product was derived from MODIS surface-reflectance data. It was provided in a sinusoidal projection at a spatial resolution of 1 km. The GLASS LAI product is produced and released by the Center for Global Change Data Processing and Analysis of Beijing Normal University (http://www.bnu-datacenter.com/). The latest version of the GLASS LAI product is version 3.0 and was used in this study.

C. Field LAI

LAI ground measurements were used in this study to validate the accuracy of the GLASS, MOD15, and GEOV1 LAI products. The LAI ground measurements were obtained using the LAI-2000 Plant Canopy Analyzer [33], by tracing the radiation and architecture of canopies [34], or by hemispherical photographs processed using the CAN_EYE software package [35]. According to guidelines defined by the CEOS/WGCV LPV subgroup, a comparison can be performed by upscaling the LAI ground measurements to the moderate-resolution products using high-resolution remotely sensed imagery [36]. An empirical transfer function between high-resolution reflectance data and LAI ground measurements for a site was established to derive a high-resolution LAI map that was then aggregated to the moderate-resolution products [13]. Forty-seven high-resolution LAI maps over 28 sites were used in this study. Detailed information about these validation sites is shown in Table I of the supplemental material. Most of the high-resolution LAI maps were reported by Garrigues *et al.* [13] and Camacho *et al.* [12]. These data mainly come from international initiatives such as VALERI (http://w3.avignon.inra.fr/valeri) and BigFoot [37]. The accuracy of these high-resolution LAI maps depends on ground measurement errors, uncertainties in the high-resolution reflectance data, and sampling and upscaling errors [38]. For high-resolution LAI maps corrected for clumping and nongreen elements, an absolute uncertainty smaller than 1 LAI unit can be expected for most sites [39].

In addition, two sites (Agro and Fermi) with a time series of LAI field measurements were selected to evaluate the seasonal changes in these LAI products. The Agro (40.01° N, 88.29° W) and Fermi (41.86° N, 88.22° W) sites are agricultural sites in the Midwestern United States that are part of the network of eddy covariance flux towers associated with AmeriFlux. Quantitative evaluation of heterogeneity using high-resolution satellite images demonstrated that the areas surrounding the Agro and Fermi sites were extremely homogeneous, which met the homogeneity requirement and minimized issues associated with spatial representativeness in point-to-pixel comparisons [40].

III. Methodology

The method proposed in this study uses GRNNs to retrieve LAI from time-series MODIS/AVHRR reflectance data. The GRNNs are trained with the fused time-series LAI from MOD15 and CYCLOPES LAI products and the preprocessed MODIS/AVHRR reflectance data over the BELMANIP sites. A rolling processing approach using the GRNNs was applied to generate a long time series of temporally continuous GLASS LAI product from the preprocessed time-series MODIS/AVHRR reflectance data. The quality and accuracy of the GLASS LAI product were evaluated. A flowchart outlining this method is shown in Fig. 1.

A. LAI Inversion From MODIS and AVHRR Reflectance Data

The method developed by Xiao *et al.* [27] was used to retrieve LAI from MODIS reflectance data in this study. The method retrieves LAI profiles from MODIS reflectance time-series data using GRNNs that were trained using the fused time-series LAI values from MOD15 and CYCLOPES LAI products and the preprocessed time-series MODIS reflectance over the BELMANIP sites. Unlike existing neural network methods that use only remote sensing data acquired at a specific time to retrieve LAI, the preprocessed MODIS reflectance data from an entire year were entered into the trained GRNNs to estimate the one-year LAI profile for each pixel [27].

Because of its excellent performance in retrieving LAI from MODIS reflectance time-series data, the method was extended in this study to estimate LAI profiles from AVHRR reflectance time-series data. A database was generated from the MOD15 and CYCLOPES LAI products as well as the preprocessed LTDR AVHRR reflectance data for the BELMANIP sites from 2003 to 2004 to train the GRNNs. For each BELMANIP site, 3×3 pixels of the preprocessed AVHRR reflectance data and the MOD15 and CYCLOPES LAI values projected into the 3×3 pixels of the preprocessed AVHRR reflectance data using the nearest-neighbor sampling technique were extracted.

Because of cloud, atmospheric, and snow contamination, the MOD15 and CYCLOPES LAI profiles exhibit time-series fluctuations during the vegetation growing seasons, and some LAI values are missing. The MOD15 and CYCLOPES LAI values were smoothed and gap filled using the multistep Savitzky–Golay (SG) filtering procedure [20]. For each data value, the SG filter fits a quadratic polynomial function to all $2k + 1$ points in a window using the least squares method, where k is the window width and is set to 5 in this study. The CYCLOPES LAI retrieval algorithm provides an effective LAI, whereas the MOD15 retrieval algorithm provides a true LAI. The clumping index derived from multiangular POLDER 3 satellite data [41] was used to convert effective CYCLOPES LAI into true LAI, which was then fused with the MOD15 LAI. The fused LAI is a linear weighted sum of the MOD15 LAI and the true

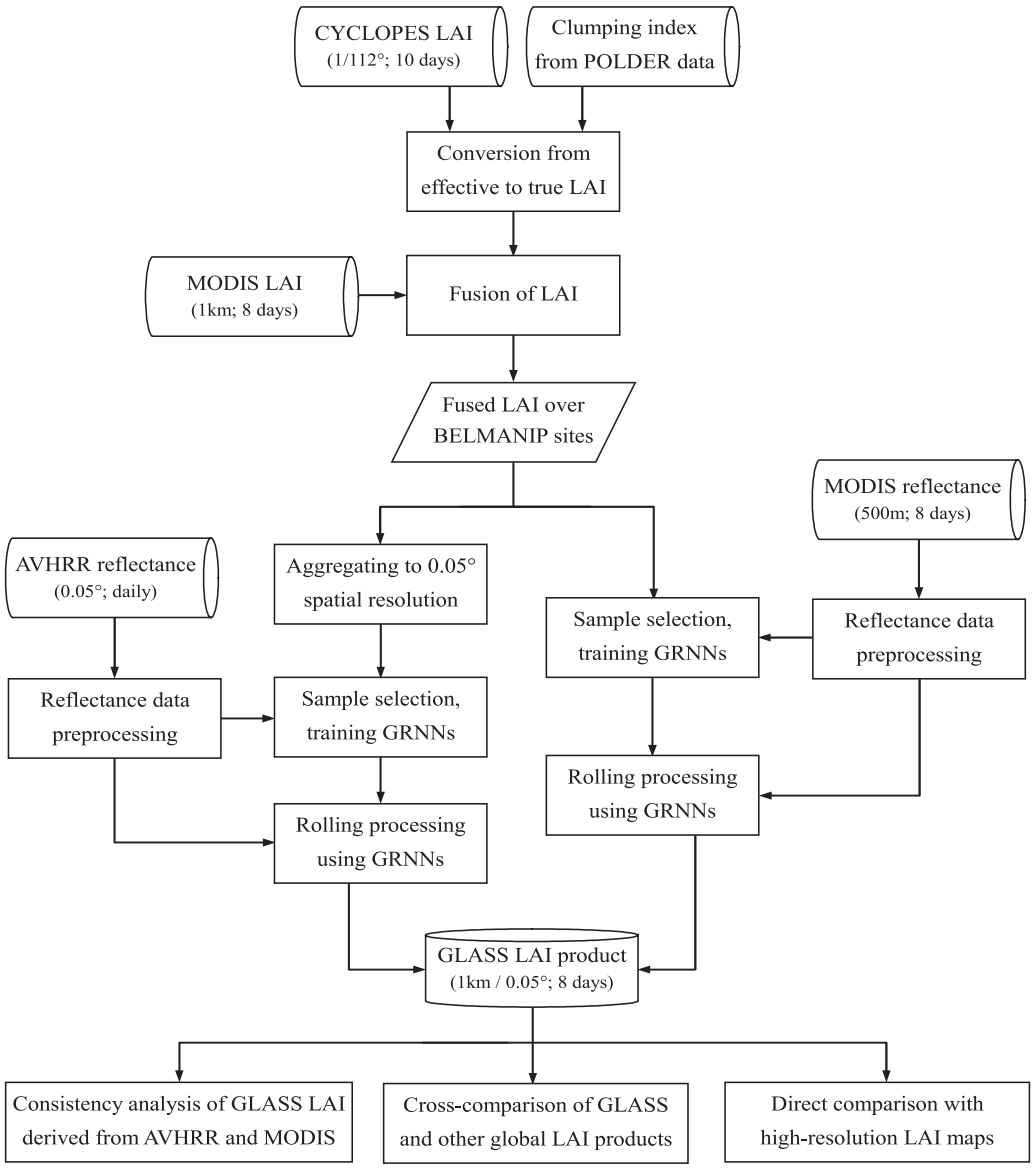

Fig. 1. Schematic description of the method used to generate the GLASS LAI product.

CYCLOPES LAI [27]. The fused LAI values were then aggregated to 0.05° spatial resolution using a spatial-average method. The average values over 0.05° pixels were computed if more than 70% of the 1-km pixels projected into the 0.05° pixels had fused LAI values.

The aggregated LAI time-series values and the corresponding preprocessed AVHRR reflectance values over the BELMANIP sites for 2003 and 2004 were used to train GRNNs. The fundamental formulation of the GRNNs with Gaussian kernel functions can be expressed as follows [42]:

$$\mathbf{Y}'(\mathbf{X}) = \frac{\sum_{i=1}^{n} \mathbf{Y}^i \exp\left(-\frac{D_i^2}{2\sigma^2}\right)}{\sum_{i=1}^{n} \exp\left(-\frac{D_i^2}{2\sigma^2}\right)} \tag{1}$$

where $D_i^2 = (\mathbf{X} - \mathbf{X}^i)^T(\mathbf{X} - \mathbf{X}^i)$ represents the squared Euclidean distance between the input vector X and the ith training input vector X^i, Y^i is the output vector corresponding to vector X^i, $Y'(X)$ is the estimate corresponding to vector X, n is the number of samples, and σ is a smoothing parameter. The input vector X of the GRNNs used to retrieve LAI profiles from the preprocessed AVHRR reflectance data includes preprocessed AVHRR time-series reflectance values in the red (R) and near-infrared (NIR) bands (for a one-year period); that is, $\mathbf{X} = (R_1, R_2, \ldots, R_{46}, \mathrm{NIR}_1, \mathrm{NIR}_2, \ldots, \mathrm{NIR}_{46})^T$ and contains 92 components. The output vector $\mathbf{Y}' = (\mathrm{LAI}_1, \mathrm{LAI}_2, \ldots, \mathrm{LAI}_{46})^T$ is the corresponding LAI time series for the year and contains 46 components. The smoothing parameter σ is the only free parameter in the GRNN formulation. Therefore, GRNN training essentially involves optimizing the smoothing parameter. In this paper, the holdout method [42] was used to find the optimal value of the smoothing parameter. The trained GRNNs were then used to retrieve LAI from the preprocessed AVHRR reflectance data. The preprocessed AVHRR reflectance data from an entire year were entered into the trained GRNNs to estimate the one-year LAI profile for each pixel.

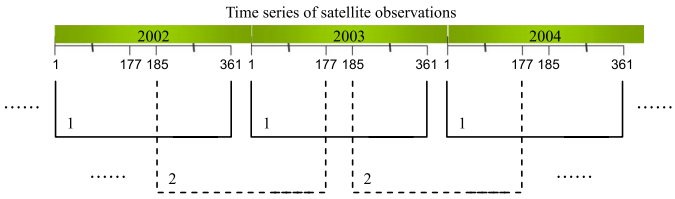

Fig. 2. Rolling processing strategy to generate temporally continuous GLASS LAI product.

B. Processing Strategy for GLASS LAI Generation

The retrieval method previously described used GRNNs to retrieve LAI profiles from MODIS and AVHRR reflectance time-series data. Although the method was used to estimate temporally continuous and smooth LAI profiles over one year, the LAI profiles of two adjacent years were not necessarily continuous. To generate a long time series of temporally continuous high-quality global LAI product using this method, a rolling processing strategy was developed in this study.

As shown in Fig. 2, two groups of GRNNs were alternately used to retrieve LAI from MODIS/AVHRR reflectance data. For the first group of GRNNs, the input vector was the preprocessed MODIS/AVHRR reflectance data for a one-year period (from Julian day 1 to 361), and the output vector was the corresponding LAI time series for the year. For the second group of GRNNs, the input vector was the preprocessed MODIS/AVHRR reflectance data from Julian day 185 of a particular year to Julian day 177 of the next year, and the output vector was the corresponding LAI time series from Julian day 185 of the particular year to Julian day 177 of the next year.

Based on the rolling processing strategy, two LAI values, respectively, denoted as LAI_1 and LAI_2, were retrieved for each point in time using the two groups of GRNNs. The GLASS LAI, which is denoted by $\mathrm{LAI}_{\mathrm{GLASS}}$, was obtained by a linear combination of LAI_1 and LAI_2 as follows:

$$\mathrm{LAI}_{\mathrm{GLASS}} = w_1 \mathrm{LAI}_1 + w_2 \mathrm{LAI}_2 \tag{2}$$

where w_1 and w_2 are the weights for LAI_1 and LAI_2, respectively. Weight w_1 was determined in this study using the following function:

$$w_1(x;a,b,c,d) = \begin{cases} 0, & x \le a \\ 2\left(\frac{x-a}{b-a}\right)^2, & a < x \le \frac{a+b}{2} \\ 1-2\left(\frac{x-a}{b-a}\right)^2, & \frac{a+b}{2} < x \le b \\ 1, & b < x \le c \\ 1-2\left(\frac{x-d}{c-d}\right)^2, & c < x \le \frac{c+d}{2} \\ 2\left(\frac{x-d}{c-d}\right)^2, & \frac{c+d}{2} < x \le d \\ 0, & x > d \end{cases} \tag{3}$$

where x represents the Julian day of the year, and a, b, c, and d are four parameters used to determine the shape of the function. The four parameters were determined so that the smallest weights were assigned to LAI values at the beginning and end of the LAI profiles (for a one-year period) and the largest weights to LAI values in the middle of the LAI profiles. In this paper, $a = 9$, $b = 169$, $c = 193$, $d = 353$, and weight w_2 was calculated as follows:

$$w_2 = 1 - w_1. \tag{4}$$

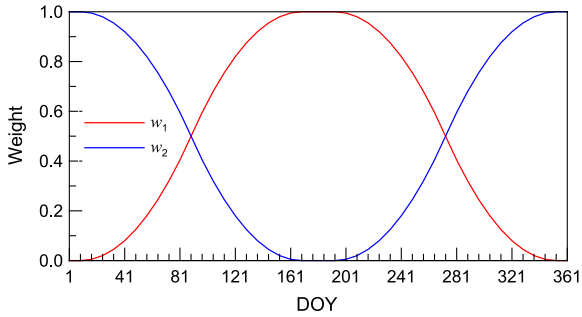

Fig. 3. Weights used to combine the LAI values retrieved using the two groups of GRNNs.

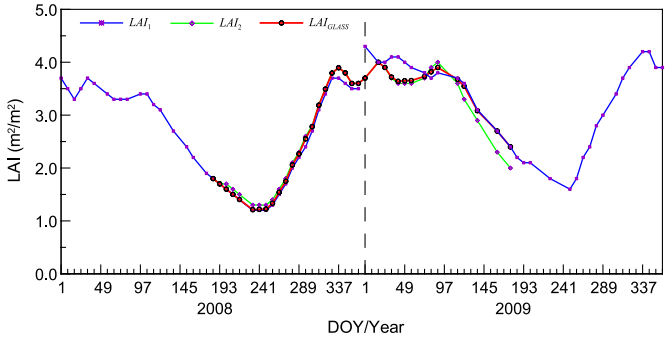

Fig. 4. Time series of GLASS LAI values obtained by a linear combination of LAI values retrieved using the two groups of GRNNs at a deciduous broadleaf forest site for 2008 and 2009.

Fig. 3 shows the curves for weights w_1 and w_2. It can be observed that the values in the middle of the LAI profiles were assigned larger weights than those on either side of the LAI profiles, whether the LAI profiles were retrieved using the first or the second group of GRNNs.

Fig. 4 shows a time series of GLASS LAI values obtained by a linear combination of the LAI values retrieved using the two groups of GRNNs at a deciduous broadleaf forest site (25.2875° S, 59.8289° W) for 2008 and 2009. At the end of 2008 and at the beginning of 2009, there was a small jump between the two LAI profiles retrieved from MODIS reflectance time-series data in 2008 and 2009, respectively, using the first group of GRNNs. At the same time, a continuous LAI profile was retrieved from MODIS reflectance time-series data from Julian days 185–361 of 2008 and Julian days 1–177 of 2009 using the second group of GRNNs. The LAI profiles retrieved using the two groups of GRNNs were combined using (2) to generate a continuous and smooth GLASS LAI profile.

C. Comparison and Validation

The LAI values derived from LTDR AVHRR reflectance data were compared with those derived from MODIS reflectance data to evaluate the consistency of GLASS LAI values based on different sensor data. A cross-comparison was performed to evaluate the spatial and temporal consistencies between the GLASS LAI product and other existing global LAI products, including MOD15 and GEOV1 LAI products. The accuracy of the GLASS LAI product was also evaluated against ground-based high-resolution LAI maps.

In this paper, only valid LAI values of these products were used for comparison and validation. For the GLASS and GEOV1 LAI products, all LAI values were considered to be

valid. For the MOD15 LAI product, the LAI values retrieved from the backup algorithm were not used for comparison and validation of the LAI products because of their overall lower quality originating from residual clouds and poor atmospheric correction [14]. In other words, only the LAI values retrieved from the main algorithm ($\mathrm{QC} < 64$) were considered to be valid.

1) Consistency of GLASS LAI Values Derived From AVHRR and MODIS Reflectance Data: To assess spatial and temporal consistencies between the LAI values derived from AVHRR reflectance data and those retrieved from MODIS reflectance data, the LAI values retrieved from MODIS reflectance data were reprojected to the geographic latitude/longitude projection used for the LAI values derived from AVHRR reflectance data using nearest-neighbor resampling and were aggregated to a resolution of 0.05° using a spatial-average method. The average values over the 0.05° pixels were computed if more than 70% of the 1-km pixels projected into the 0.05° pixels had valid LAI values.

A histogram comparison between the LAI values derived from MODIS reflectance data and those derived from AVHRR reflectance data from Julian day 185 in 2003 to Julian day 177 in 2004 was performed for each of the eight vegetation classes according to the MODIS land-cover type climate modeling grid product (MCD12C1). Month-by-month spatial differences between LAI values derived from AVHRR reflectance data and those derived from MODIS reflectance data were analyzed across different biomes for the one-year period. The LAI differences were calculated by subtracting the LAI values derived from MODIS reflectance data from those derived from AVHRR reflectance data.

To show the consistency of the time-series trends in the GLASS LAI values derived from MODIS and AVHRR reflectance data, the annual anomalies of the GLASS LAI values were calculated by subtracting the long-term mean from the mean annual LAI. The long-term mean in this study was the arithmetic mean of all mean annual LAI values from 1982 to 2012. In addition, LAI profiles from 1982 to 2012 over several sites with different land-cover types were also analyzed to check the temporal consistency of the GLASS LAI values derived from MODIS and AVHRR reflectance data.

2) Cross-Comparison of GLASS and Other Global LAI Products: For comparisons of spatial consistency, the GLASS, MOD15, and GEOV1 LAI products were, respectively, aggregated into a monthly time step by computing a monthly average from the valid LAI values of each month. The global maps of mean LAI for these LAI products in January and July for 2001–2010 were computed to investigate spatial patterns specific to a given product as well to check the distribution in space of the missing data. Histograms of the GLASS, MOD15, and GEOV1 LAI products for 2001–2010 were generated for each biome type according to the MODIS land-cover type product (MCD12Q1) to analyze the similarities and differences among these LAI products.

To compare temporal consistency, the original temporal resolution for each LAI product was considered. Temporal profiles of the GLASS, MOD15, and GEOV1 LAI products were checked over a sample of sites (Table I of the supplemental material) with different biome classes. To reduce the effects of coregistration errors among these LAI products and the inconsistencies associated with differences in the point-spread function of the reprojected products, the average LAI profiles over 3×3 pixels centered on selected sites were calculated if more than five of the nine pixels had valid LAI values [12]. For each site, the average LAI profiles over three consecutive years were compared to provide a qualitative analysis of the seasonal variations among these LAI products. The specific years used for comparison were not the same for all sites, but varied somewhat based on the availability of high-resolution LAI maps derived from ground measurements. These LAI profiles were also compared with the mean values of the high-resolution LAI maps over the 3 km $\times$ 3 km regions centered on the location of each site to analyze the precision of each product in the time series. The LAI temporal profiles at the center pixel of the Agro and Fermi sites were compared with the time series of LAI field measurements to evaluate the seasonal changes in these LAI products.

With respect to the process of vegetation succession, LAI continuously varies with time except in the case of disturbances such as fires, floods, and hurricanes. Therefore, a smooth temporal course of LAI products derived from remote sensing data can be expected [15]. Currently, temporal smoothness is one of the most important measures of temporal consistency. As suggested by Weiss *et al.* [15], the absolute value of the difference between the center value for three consecutive product dates in the time series and the average value corresponding to two adjacent dates, which is denoted by δLAI, was computed to quantify the smoothness of the GLASS, MOD15, and GEOV1 LAI products in this study. The smoother the temporal profiles, the smaller the δLAI values should be.

3) Direct Validation: The GLASS, MOD15, and GEOV1 LAI products were compared with the same set of high-resolution LAI maps to evaluate differences in LAI magnitude among these products. The high-resolution LAI maps and the GLASS, MOD15, and GEOV1 LAI products were aggregated over 3 km $\times$ 3 km regions centered on the location of the validation sites using the spatial-average method, and the GLASS, MOD15, and GEOV1 LAI values were linearly interpolated to the acquisition date of a LAI ground measurement if the two closest LAI values were within ± 10 days of this date. A total of 48 sites were finally retained and provided 64 ground-based LAI measurements for which all the GLASS, GEOV1, and MOD15 LAI products provide valid LAI values. The discrepancies of each product were quantified by the coefficient of determination, R-squared (R^2), root mean square error (RMSE), and the mean (μ) and standard deviation (σ) of the difference between these LAI products and the high-resolution LAI maps.

IV. Results

A. Consistency of GLASS LAI Values Derived From AVHRR and MODIS Reflectance Data

Fig. 5 shows a histogram comparison between the GLASS LAI values derived from MODIS reflectance data and those derived from AVHRR reflectance data from Julian day 185

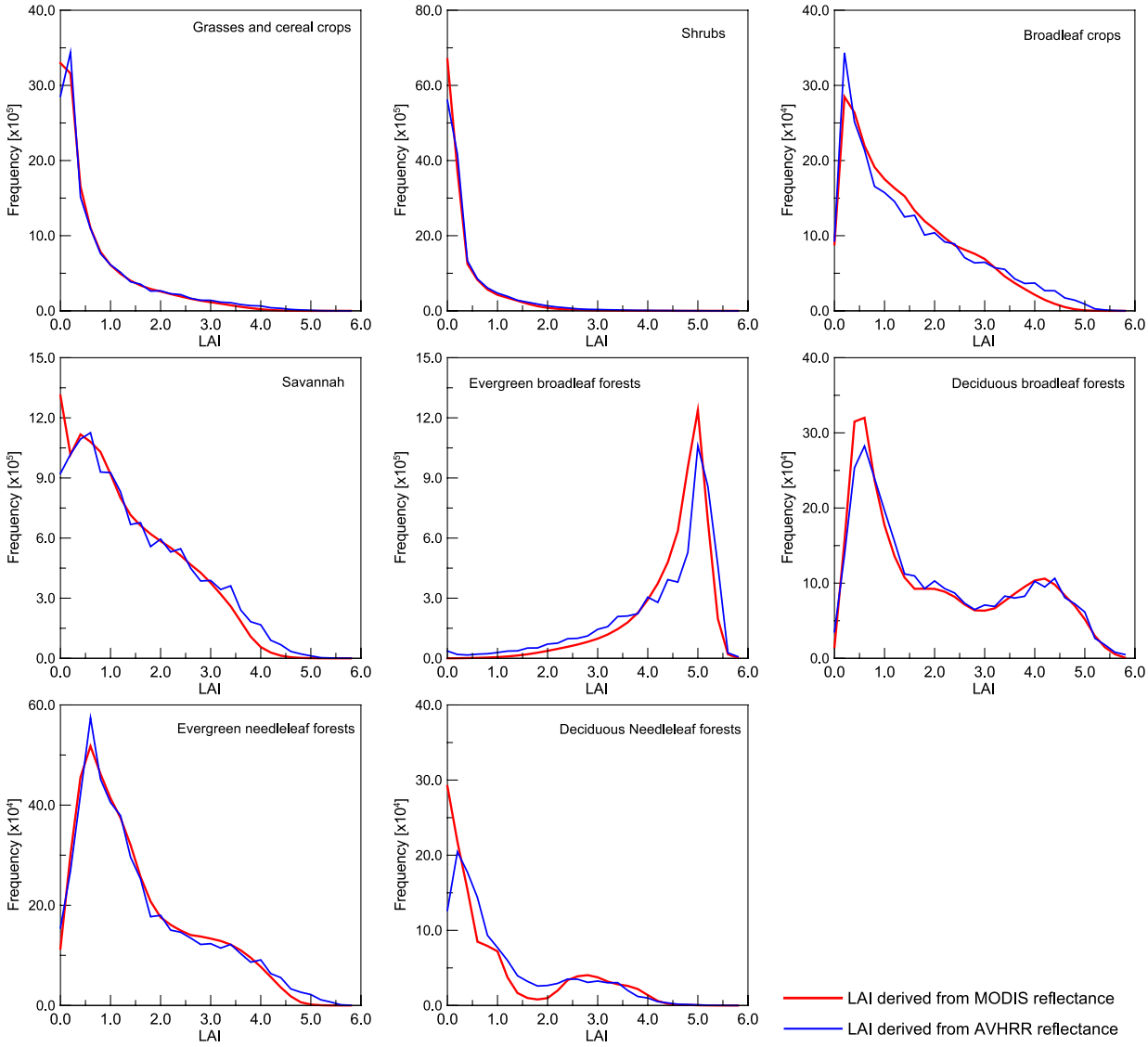

Fig. 5. Statistical distributions of global LAI values derived from MODIS reflectance data and those derived from AVHRR reflectance data from Julian day 185 in 2003 to Julian day 177 in 2004 for different vegetation classes.

in 2003 to Julian day 177 in 2004 for each of the eight vegetation classes according to the MCD12C1 product. This comparison indicates that the distributions of GLASS LAI values derived from AVHRR and MODIS reflectance data are consistent with one another for each biome, particularly for the grass/cereal crop, shrub, and deciduous broadleaf forest biome types. At larger LAI values, the frequencies of GLASS LAI values derived from AVHRR reflectance data showed slightly higher values in the broadleaf crop, savannah, and evergreen needleleaf forest biome types. GLASS LAI values derived from AVHRR reflectance data were slightly underestimated relative to GLASS LAI values derived from MODIS reflectance data for evergreen broadleaf forest. For deciduous needleleaf forest, the frequencies of GLASS LAI values derived from MODIS reflectance data were slightly larger when the LAI values were less than 0.5 and slightly smaller when the GLASS LAI values were between 0.5 and 2.5, compared with the frequencies of GLASS LAI values derived from AVHRR reflectance data.

Table II shows the mean values and standard deviations of the LAI differences for different biomes and for the 12 months from Julian day 185 in 2003 to Julian day 177 in 2004. The mean values of the LAI differences were less than 0.3 for each biome for all 12 months. The LAI values derived from AVHRR reflectance data were larger than those derived from MODIS reflectance data by almost 0.2 LAI units for the grass/cereal crops, shrubs, broadleaf crops, and savannah biome types, whereas the LAI values derived from AVHRR reflectance data were lower than those derived from MODIS reflectance data by almost 0.3 LAI units for evergreen broadleaf forest. The last row in Table II shows the mean values and standard deviations of LAI differences between the annual maximum LAI values derived from AVHRR reflectance data and those derived from MODIS reflectance data from Julian day 185 in 2003 to Julian day 177 in 2004 across different biomes, which reflect the worst possible case. It can be observed that the mean values of LAI differences calculated from annual maximum LAI values are less than 0.3 and the standard deviations are less than 1.0 for most vegetation classes. Evergreen broadleaf forest has the largest mean value and standard deviation. In this vegetation type, the LAI values derived from MODIS reflectance data were larger than those

TABLE II
ANALYSIS OF LAI DIFFERENCES BETWEEN LAI VALUES DERIVED FROM AVHRR REFLECTANCE DATA AND THOSE DERIVED FROM MODIS REFLECTANCE DATA ACROSS DIFFERENT BIOMES FOR 12 MONTHS AND FOR ANNUAL MAXIMUM LAI DIFFERENCES FROM JULIAN DAY 185 IN 2003 TO JULIAN DAY 177 IN 2004

Year	Month	GCC		SHB		BLC		SVN		EBF		DBF		ENF		DNF	
		M	SD	M	SD	M	SD	M	SD	M	SD	M	SD	M	SD	M	SD
2003	Jul	0.08	0.476	0.057	0.427	0.125	0.569	0.142	0.513	-0.261	0.939	-0.105	0.575	-0.071	0.64	-0.252	0.559
2003	Aug	0.063	0.452	0.07	0.376	0.087	0.558	0.139	0.478	-0.255	0.958	-0.078	0.598	-0.026	0.589	-0.136	0.485
2003	Sep	0.065	0.36	0.084	0.31	0.104	0.529	0.135	0.437	-0.255	0.929	0.003	0.558	0.029	0.503	0.18	0.343
2003	Oct	0.052	0.3	0.09	0.328	0.125	0.52	0.16	0.453	-0.204	0.934	0.087	0.456	0.085	0.513	0.235	0.364
2003	Nov	0.044	0.298	0.074	0.347	0.113	0.518	0.165	0.469	-0.177	0.94	0.094	0.454	0.077	0.54	0.169	0.363
2003	Dec	0.049	0.293	0.065	0.331	0.082	0.496	0.127	0.443	-0.277	0.932	0.066	0.443	0.097	0.531	0.173	0.334
2004	Jan	0.046	0.301	0.064	0.34	0.059	0.513	0.113	0.44	-0.217	0.931	0.048	0.424	0.063	0.539	0.168	0.34
2004	Feb	0.044	0.292	0.069	0.335	0.044	0.521	0.107	0.423	-0.206	0.896	0.044	0.402	0.065	0.536	0.155	0.351
2004	Mar	0.049	0.28	0.071	0.331	0.029	0.483	0.1	0.409	-0.27	0.876	0.055	0.388	0.076	0.514	0.156	0.344
2004	Apr	0.075	0.319	0.074	0.358	0.045	0.519	0.131	0.446	-0.258	0.881	0.049	0.459	0.047	0.542	0.145	0.382
2004	May	0.097	0.378	0.059	0.381	0.079	0.566	0.138	0.471	-0.234	0.897	-0.054	0.55	-0.006	0.555	0.023	0.403
2004	Jun	0.13	0.489	0.06	0.423	0.087	0.588	0.152	0.506	-0.245	0.937	-0.013	0.627	-0.028	0.638	-0.125	0.516
Annual maximum LAI		0.225	0.69	0.152	0.618	0.227	0.891	0.259	0.762	-0.424	1.327	0.001	0.941	0.042	0.96	-0.104	0.823

GCC = Grasses and cereal crops. SHB = Shrubs. BLC = Broadleaf crops. SVN = Savannah. EBF = Evergreen broadleaf forests. DBF = Deciduous broadleaf forests. ENF = Evergreen needleleaf forests. DNF = Deciduous needleleaf forests.
M = mean value of the LAI difference.
SD = standard deviation of the LAI difference.

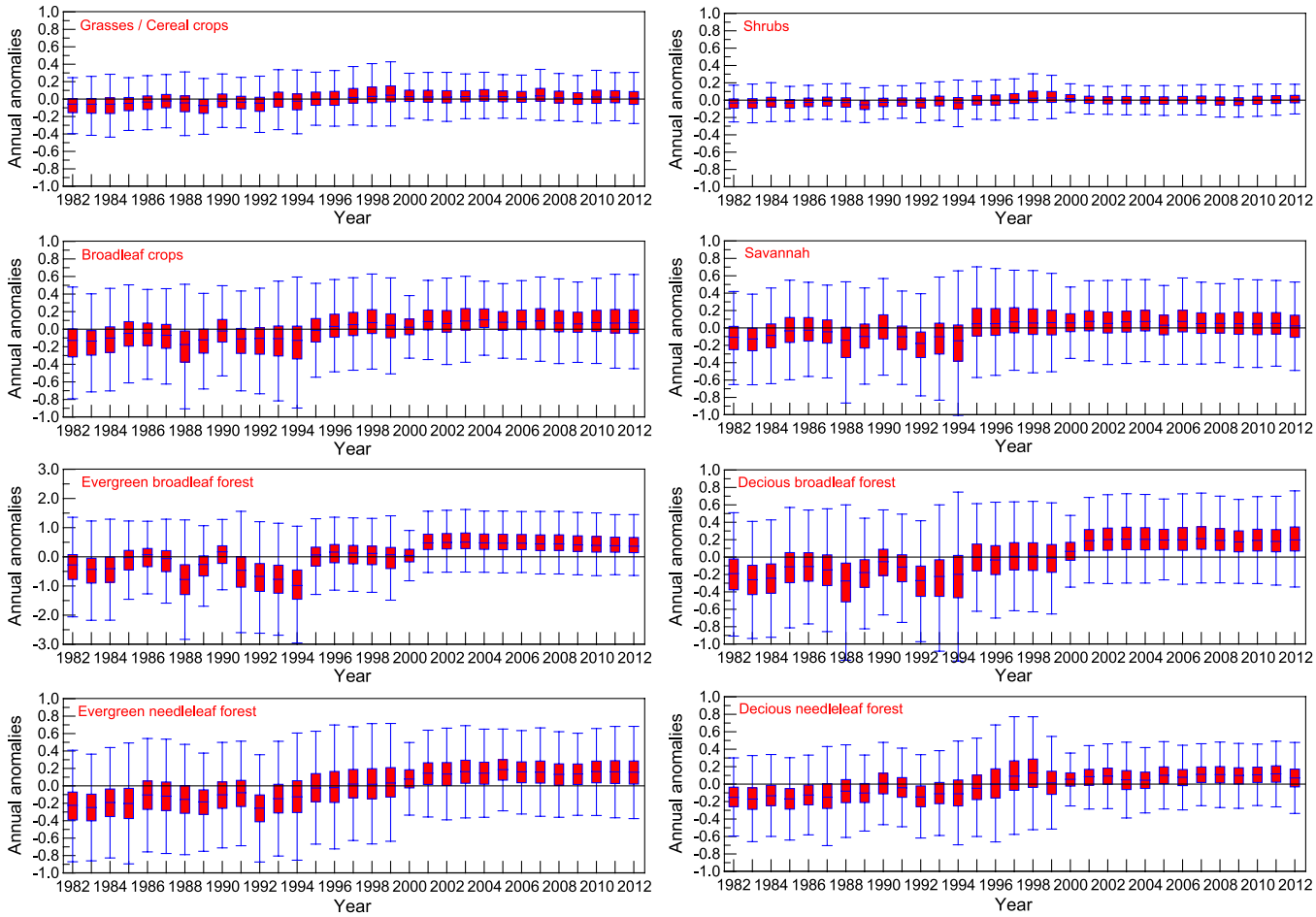

Fig. 6. Box plots of annual anomalies of the GLASS LAI product during 1982–2012 for different vegetation classes. Each box stretches from the 25th percentile to the 75th percentile. Outliers located more than one and one-half times the length of the box from either end of the box are not displayed.

derived from AVHRR reflectance data by almost 0.43 LAI units. The lower LAI values derived from AVHRR reflectance data corresponded to poor-quality AVHRR reflectance data caused by persistent cloud contamination [25]. Overall, the difference values indicate spatiotemporal agreement between LAI values derived from AVHRR reflectance data and those derived from MODIS reflectance data.

Fig. 6 shows box plots of the annual anomalies for various vegetation classes according to the MCD12C1 product. Generally, the median values of the LAI annual anomalies are close to zero and show a continuous increasing trend for all biomes except for evergreen broadleaf forest. For evergreen broadleaf forest, the annual anomalies of GLASS LAI values derived from MODIS reflectance data were relatively

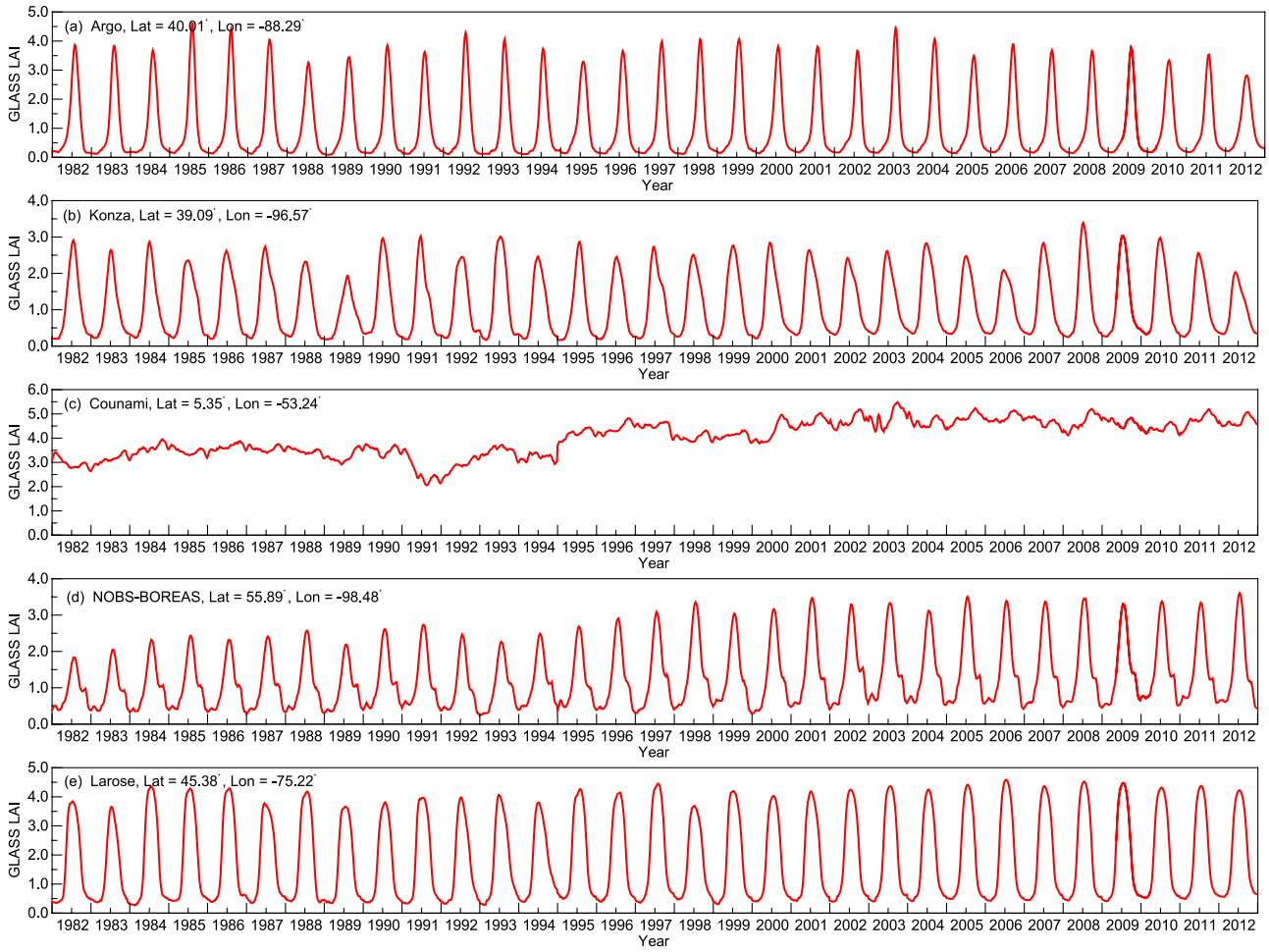

Fig. 7. Temporal profiles of GLASS LAI over five sites with different vegetation types from 1982 to 2012.

smooth. In contrast, small fluctuations were observed in the annual anomalies of GLASS LAI values derived from AVHRR reflectance data. This occurred because the quality of the MODIS surface-reflectance data was significantly better than that of the AVHRR surface-reflectance data over tropical forest regions [25]. Furthermore, several months of AVHRR data were missing in 1994 because of the late overpass of NOAA-14. In summary, the GLASS LAI product derived from MODIS and AVHRR reflectance data had very good consistency for time-series trend analysis.

Fig. 7 shows the time series from the GLASS LAI product for the Agro, Konza, Counami, NOBS-BOREAS NSA, and Larose sites during 1982–2012. Detailed information about these sites is given in Table I of the supplemental material. The plots indicate that the GLASS LAI derived from AVHRR and MODIS reflectance data had good temporal consistency and that the GLASS LAI product was able to capture the seasonal change properties of vegetation.

B. Cross-Comparison of GLASS LAI and Other Global LAI Products

1) Spatial Consistency: Spatial distribution maps of global mean LAI for the GLASS, MOD15, and GEOV1 LAI products in January and July during 2001–2010 are shown in Fig. 8. Areas masked in gray (see Fig. 8) correspond to pixels where these LAI products did not provide a valid LAI value. The MOD15 and GEOV1 LAI products contain many missing pixels in rainforest regions and in middle- and high-latitude zones of the Northern Hemisphere, particularly in January. Camacho *et al.* [12] reported that the percentage of missing values at high latitudes in the Northern Hemisphere varied as a function of the period of the year (it reached a maximum in winter), mainly due to snow coverage changes throughout the year as well as an increase in observations under dark conditions, particularly above the Arctic Circle in winter. As a consequence of more prevalent cloudiness, the GEOV1 and MOD15 LAI products also presented a large fraction of gaps (up to 50% and 60%, respectively) over the Equatorial region [12]. However, no missing values existed in the GLASS LAI product. This can be attributed to the GLASS LAI retrieval algorithm, which uses surface reflectance for a one-year period as its input to estimate a one-year LAI profile for each pixel and a series of preprocessing tasks to produce improved algorithm inputs.

It is apparent that the GLASS, MOD15, and GEOV1 LAI products are generally consistent in their spatial patterns (see Fig. 8). The Northern and Southern Hemispheres clearly showed opposite seasonality. These LAI products presented their highest values over Equatorial forest. LAI values were intermediate at middle- and high-latitude zones, and all products showed small LAI peaks and high variability around

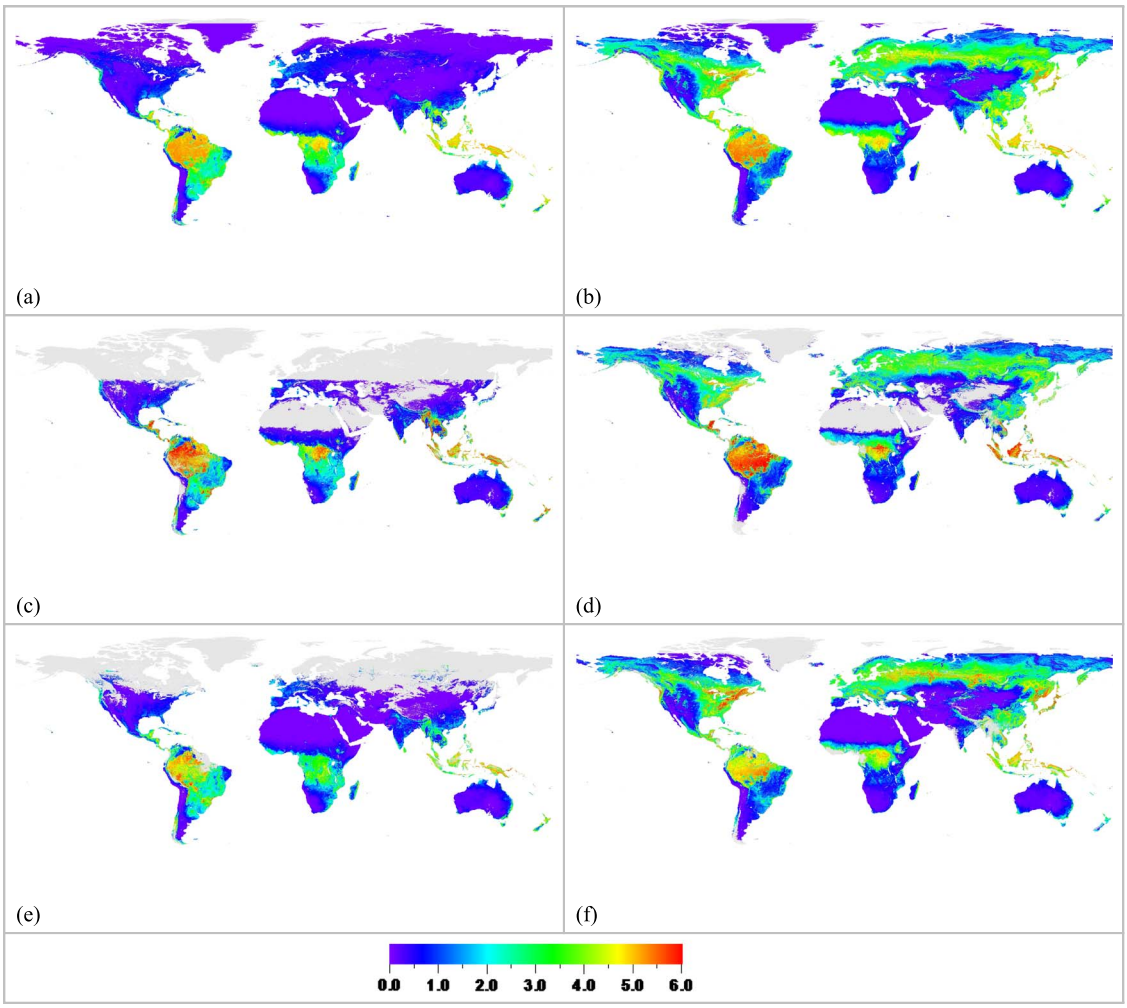

Fig. 8. Global mean LAI for GLASS, MOD15, and GEOV1 products in (left) January and (right) July over 2001–2010. Geographic latitude/longitude projection, 0.05° resolution for display purposes. (a) GLASS, January. (b) GLASS, July. (c) MOD15, January. (d) MOD15, July.

50° N–60° N in July. LAI values were very low over sparsely vegetated areas. However, discrepancies existed in the magnitudes of these LAI products. At middle and high latitudes of the Northern Hemisphere, these LAI products were more consistent in January than in July. The GLASS and GEOV1 LAI values were between 0.5 and 1.0 LAI units higher than the MOD15 LAI values around 50° N–60° N in July. In the Southern Hemisphere, these LAI products were in good agreement, particularly in July. A relatively large discrepancy among these LAI products was observed in tropical forest regions. The MOD15 LAI values over these regions could reach 6.8 LAI units and were larger than the corresponding GLASS LAI values, which was partly due to overestimation of the MOD15 LAI values associated with broadleaf forests [13]. The GEOV1 LAI values were lower than the GLASS and MOD15 LAI values in these regions, particularly in January. The largest difference between the GEOV1 and GLASS LAI values in these regions was as much as 1.5 LAI units.

Histograms of the GLASS, MOD15, and GEOV1 LAI products from 2001 to 2010 for each biome type according to the MCD12Q1 product are shown in Fig. 9. Among the biome classes, the three LAI products for grasses/cereal crops and shrubs demonstrated the most consistent distributions. Some discrepancies among these LAI products were observed for broadleaf crops, savannah, deciduous broadleaf forest, and evergreen needleleaf forest. For very low LAI values, the frequencies of the GEOV1 product showed the highest values; as LAI values increased, the frequencies of the MOD15 LAI product showed the highest values; for the highest LAI values, the GLASS LAI product showed the highest frequencies.

Larger discrepancies were apparent for evergreen broadleaf forests and deciduous needleleaf forests. For the evergreen broadleaf forest biome type, the GLASS LAI values exhibited a distribution with a narrow peak at approximately 5.0, and the peak position of the MOD15 LAI frequency distribution was approximately 5.7. The GEOV1 LAI values showed a distribution closer to that of the GLASS LAI values, but the frequencies of the GEOV1 LAI values showed a more even distribution because the GEOV1 LAI product typically presents lower values for this biome type [43].

2) Temporal Consistency: For each of the main biome classes according to the MCD12Q1 product, three sites were selected to illustrate the seasonality of the GLASS, MOD15, and GEOV1 LAI products (see Fig. 10). Fig. 10(a) shows temporal LAI trajectories over the Konza, Tundra, and Sud-Ouest sites. The biome type for these sites is grasses and

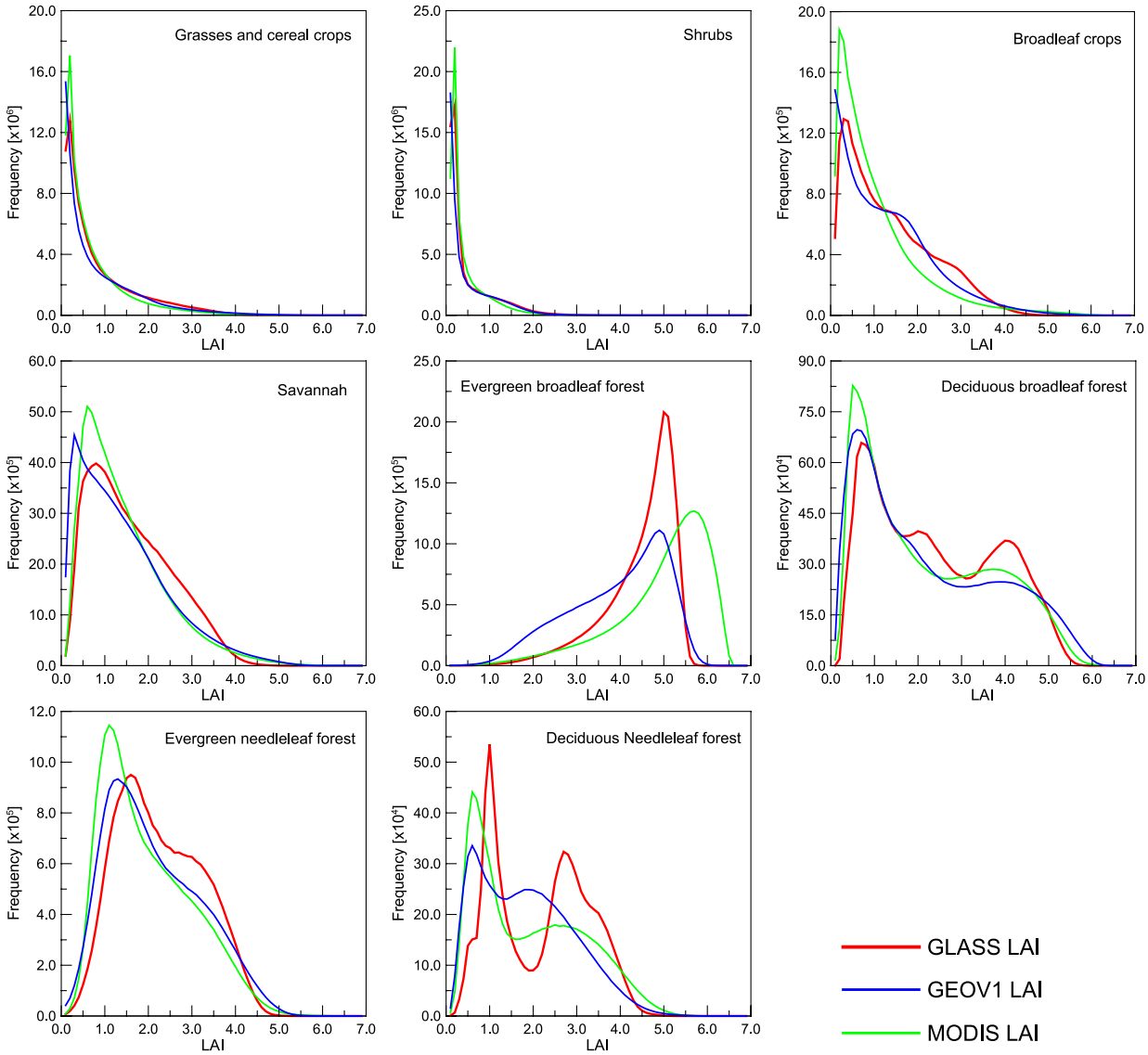

Fig. 9. Histograms of the GLASS, MOD15, and GEOV1 LAI products for 2001–2010 for different biome types.

cereal crops. Over the Konza site, the GLASS, MOD15, and GEOV1 LAI products captured similar temporal trajectories. The GLASS and GEOV1 products yielded smooth LAI profiles. The MOD15 LAI values were between 0.5 and 0.8 higher than those of GLASS and GEOV1 at the peak of each growing season in 2000 and 2002. Over the Tundra site, the GLASS LAI profile was complete, but most of the GEOV1 and MOD15 LAI values were missing, particularly during nongrowing seasons. The GEOV1 and MOD15 LAI profiles maintained lower LAI values than the GLASS LAI profile. The GLASS LAI values were slightly underestimated, with values lower by 0.2 LAI units than the mean value of the high-resolution LAI map at this site. Over the Sud-Ouest site, the GLASS LAI profile was in good agreement with the GEOV1 LAI profile during these years. The MOD15 LAI values were much lower than the GLASS and GEOV1 LAI values, particularly during the growing seasons over this site. The agreement of the GLASS and GEOV1 LAI values with the mean value of the high-resolution LAI map was very good. Compared with this mean value, the GEOV1 LAI values were slightly underestimated by 0.1 LAI units, whereas the GLASS LAI values were overestimated by less than 0.2 LAI units.

Fig. 10(b) shows temporal LAI trajectories over the Argo, Barrax, and Demmin sites with the broadleaf crop biome type. Over the Argo site, all LAI profiles exhibited consistent seasonal variations. The GLASS, MOD15, and GEOV1 LAI values demonstrated excellent agreement during nongrowing seasons, but the GEOV1 LAI values were generally larger than the GLASS and MOD15 LAI values during growing seasons. Similar results were observed at the Barrax site, where the GEOV1 LAI values were higher than the GLASS and MOD15 LAI values (by up to 0.5 LAI units) during growing seasons. The GLASS and MOD15 LAI values were in good agreement with the mean value of the high-resolution LAI map in 2004, but the GLASS and MOD15 LAI values were slightly overestimated (by 0.1–0.2 LAI units) compared with the mean value of the high-resolution LAI map in 2005. Over the Demmin site, good agreement was observed among the GLASS, MOD15,

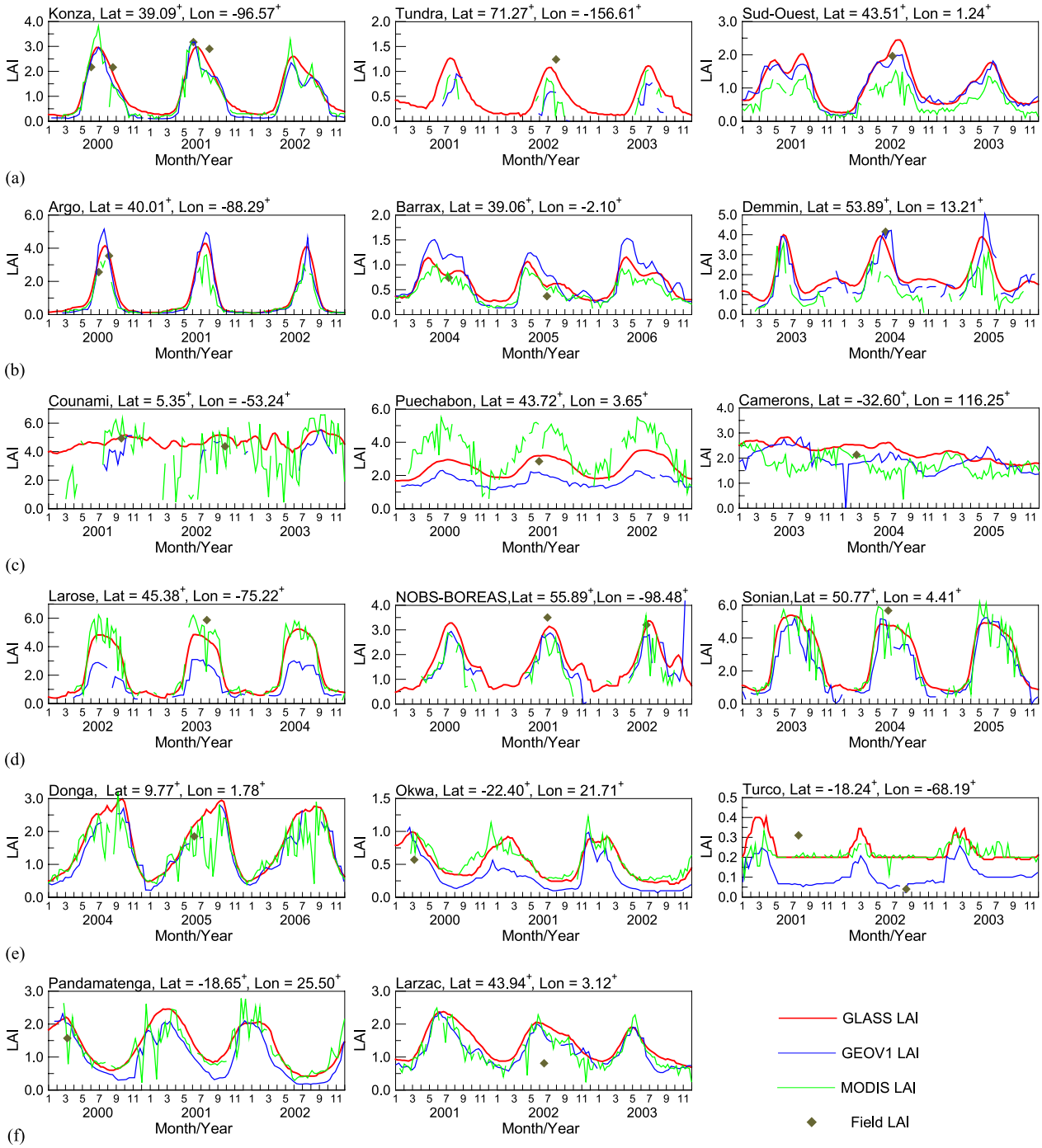

Fig. 10. Temporal profiles of GLASS, MOD15, and GEOV1 LAI values over a sample of sites with different biome classes. (a) Grasses and cereal crops. (b) Broadleaf crops. (c) Broadleaf forests. (d) Needleleaf forests. (e) Shrub. (f) Savannah.

and GEOV1 LAI values for 2003. The GLASS and MOD15 LAI profiles exhibited consistent seasonal variations, but the GEOV1 LAI profile showed a phase lag when compared with the GLASS and MOD15 LAI profiles during the growing season in 2004–2005, when the GLASS and GEOV1 LAI values were between 1.0 and 2.0 LAI units higher than the MOD15 LAI values.

Fig. 10(c) presents temporal LAI trajectories over broadleaf forest sites. Over the Counami site, the biome type is evergreen broadleaf forest. Most of the GEOV1 LAI values were missing. The temporal profile of MOD15 LAI values at this site was very noisy, which could be partly due to the high sensitivity of MOD15 LAI values to surface-reflectance uncertainties for large LAI values [44]. In contrast, the GLASS LAI product captured a complete and reasonable temporal profile that was relatively smooth and exhibited limited seasonality. Meanwhile, the GLASS LAI values were generally in good agreement with the mean values of high-resolution LAI maps. Over the Puechabon site, the GLASS, MOD15, and GEOV1 LAI values exhibited similar temporal trajectories, but large discrepancies could be observed in LAI magnitudes among these LAI products for each year. The GLASS LAI values were generally

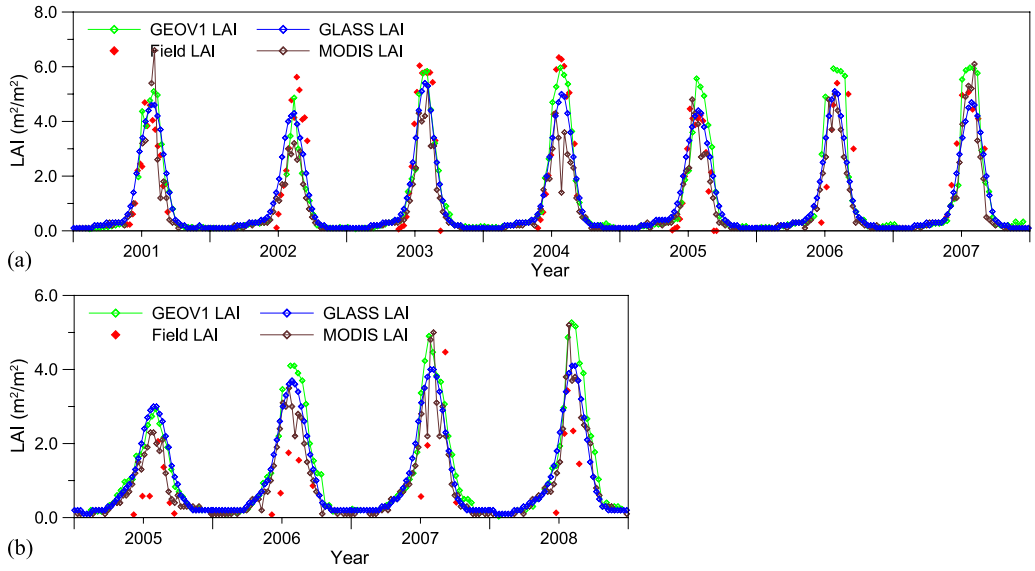

Fig. 11. Temporal profiles of GLASS, MOD15, and GEOV1 LAI values over the (a) Agro and (b) Fermi sites with time series of LAI field measurements.

between the MOD15 and GEOV1 LAI values: The MOD15 LAI values, except for dramatic fluctuations, were between 1.0 and 2.0 LAI units larger than the GLASS LAI values during growing seasons in these years, whereas the GEOV1 LAI values were systematically lower than the GLASS LAI values (up to 1.5 LAI units). The GLASS LAI values outperformed the LAI values of other products in terms of accuracy compared with the mean value of the high-resolution LAI map at this site. The Camerons site is a dry evergreen broadleaf forest site. Similarly to the Counami site, the GLASS LAI profile as well as the GEOV1 and MOD15 LAI profiles at this site presented almost no seasonality, as expected for these evergreen forests, and which is consistent with the findings of Camacho *et al.* [20].

The temporal profiles of the GLASS, MOD15, and GEOV1 LAI values over the Larose, NOBS-BOREAS, and Sonian sites with the needleleaf forest biome type are provided in Fig. 10(d). Over the Larose site, the land cover is composed mainly of boreal forest (conifers and deciduous trees) and wetland (grass and shrubs). All the LAI products showed similar seasonal and interannual variability, although with considerable differences in magnitude. The GEOV1 LAI values were significantly lower than the GLASS and MOD15 LAI values (by up to 2.0 LAI units) during each growing season. The NOBS-BOREAS site is predominantly forested with black spruce stands of variable density, but contains numerous wetlands, small open-water bodies, small aspen stands, and extensive moss cover [45]. The GEOV1 and MOD15 LAI values were missing for the winters because of large uncertainties in the reflectance data. The GLASS LAI values were slightly higher than those of MOD15 and GEOV1 in 2000–2001 and were closer to the mean values of the high-resolution LAI maps at this site. Over the Sonian sites, all the products showed similar seasonal and interannual variations and had almost the same magnitude, although the MOD15 LAI profile showed dramatic fluctuations during the growing seasons in 2003–2005.

As for the shrub biome type, the LAI temporal profiles over the Donga, Okwa, and Turco sites are shown in Fig. 10(e). Over the Donga site, the GLASS and GEOV1 LAI profiles achieved good agreement with the envelope of the time-series MOD15 LAI values, although many of the GEOV1 LAI values were missing during the peak of each growing season. Over the Okwa site, the GLASS and MOD15 LAI profiles had almost the same magnitude, whereas the GEOV1 LAI profile presented lower magnitude throughout these years. Over the Turco site, the GLASS, MOD15, and GEOV1 LAI profiles all showed good completeness. The LAI values for all three LAI products were less than 0.5 during these years. Excellent agreement was achieved between the GLASS and MODIS LAI profiles at this site. The GEOV1 LAI values were systematically lower than those of MOD15 and GLASS (up to 0.15 LAI units) throughout these years.

Fig. 10(f) shows temporal LAI trajectories over the Pandamatenga and Larzac sites, which are of the savannah biome type. Over the Pandamatenga site, the GLASS, MOD15, and GEOV1 LAI profiles showed similar temporal trajectories, but the GEOV1 LAI values were lower than the GLASS and MOD15 LAI values during the nongrowing season of each year. Over the Larzac site, all these LAI products were in good agreement, and the LAI values of these products were all overestimated by 0.8–1.2 LAI units compared with the mean value of the high-resolution LAI map.

Fig. 11 shows the temporal profiles of GLASS, MOD15, and GEOV1 LAI values over the Agro and Fermi sites to evaluate the seasonal changes of these LAI products. For comparison, the time series of LAI field measurements is also displayed in Fig. 11. The GLASS, MOD15, and GEOV1 LAI profiles showed similar seasonal and interannual variability, although there were some discrepancies in LAI magnitude, particularly at the peak of each growing seasons. At the Agro site, the seasonal change patterns exhibited by the GLASS, MOD15, and GEOV1 LAI values were in good agreement with that of the time series of LAI field measurements [see Fig. 11(a)]. All the satellite-based LAI values consistently underestimated the field measurements at the peak of the growing season in 2002, which may be partly explained by errors as well as the scale mismatch of the field measurements. At the Fermi site, the

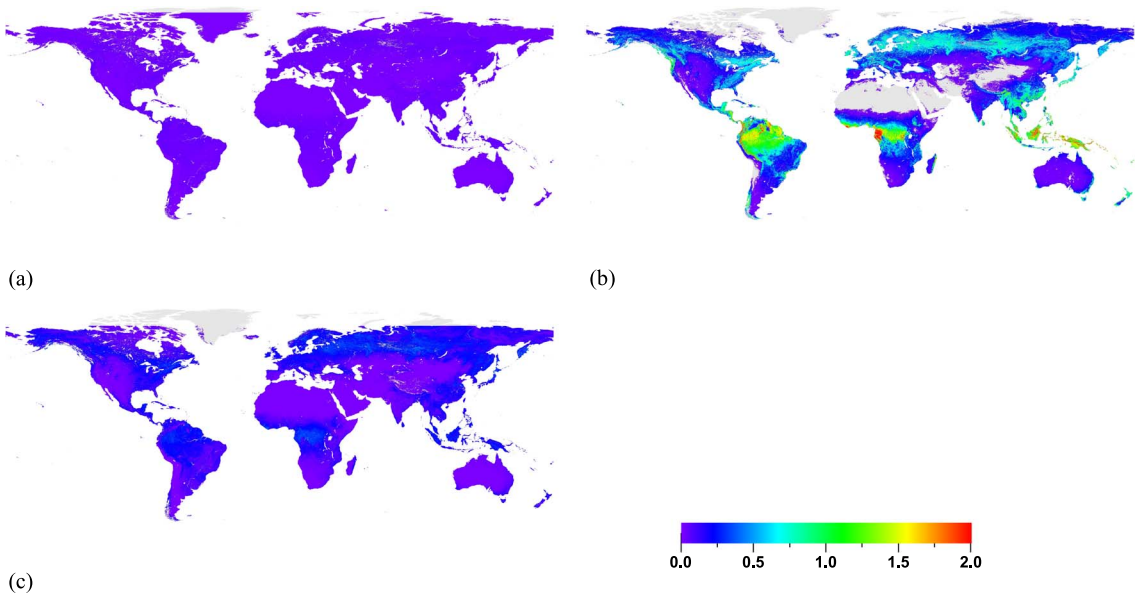

Fig. 12. Maps of mean δLAI for GLASS, MOD15, and GEOV1 LAI products over 2001–2010. Geographic latitude/longitude projection, 0.05° resolution for display purposes. (a) GLASS. (b) MOD15. (c) GEOV1.

growing seasons according to GLASS, MODIS, and GEOV1 LAI values were significantly advanced compared with the seasonality exhibited by the time series of LAI field measurements [see Fig. 11(b)], which resulted in the GLASS, MODIS, and GEOV1 LAI values being higher than the field-measured LAI values before the peak of each growing season.

Fig. 12 shows mean δLAI maps for the GLASS, MOD15, and GEOV1 LAI products from 2001 to 2010. Obviously, the GLASS product has the smallest δLAI values (< 0.1) for different vegetation types around the world, which demonstrates that the GLASS LAI product has the smoothest temporal profiles because the GLASS LAI algorithm estimates one-year LAI profiles from the preprocessed reflectance data for a one-year period: The possible noise is smoothed out. The δLAI values for the MOD15 LAI products are clearly higher than those for the GLASS and GEOV1 LAI products, particularly in rainforest regions along the Equator, with δLAI values greater than 1.0. These quantitative results confirm the qualitative observations of the temporal profiles over the selected sites shown in Fig. 10.

C. Direct Validation

The scatterplots in Fig. 13 show the GLASS, GEOV1, and MOD15 LAI values versus the mean values of the high-resolution LAI maps over the validation sites shown in Table I of the supplemental material. The relationships between the GLASS, GEOV1, and MOD15 LAI values and the mean values of the high-resolution LAI maps had slopes of 0.7418, 0.6582, and 0.5969, respectively, and positive intercepts (0.2753, 0.2511, and 0.2494), which means that the GLASS, GEOV1, and MOD15 LAI values overestimated the mean values of the high-resolution LAI maps when LAI values were low and underestimated them when LAI values were high. Compared with the MOD15 LAI values, the GLASS and GEOV1 LAI values are distributed more closely around the 1:1 line with the mean values of the high-resolution LAI maps, which demonstrates that the GLASS and GEOV1 LAI products achieved better agreement across the whole range of LAI values than the MOD15 LAI product. However, the GLASS LAI values were in slightly better agreement with the mean values of the high-resolution LAI maps than the GEOV1 LAI values, particularly for the highest LAI values, although a slight underestimation of the highest values over forest can be observed for the GLASS LAI product.

A comparison of these scatterplots with the high-resolution LAI maps indicates that the performance of the GLASS LAI product (RMSE $= 0.7848$, $\mu = -0.2172$, and $\sigma = 0.7761$) was better than those of the GEOV1 LAI product (RMSE $= 0.9084$, $\mu = -0.4008$, and $\sigma = 0.8152$) and the MOD15 LAI product (RMSE $= 1.1173$, $\mu = -0.5193$, and $\sigma = 0.9963$). The GLASS LAI values also provided the highest R-squared value ($R^2 = 0.8095$) against the mean values of the high-resolution LAI maps compared with the GEOV1 ($R^2 = 0.7939$) and MOD15 ($R^2 = 0.6705$) LAI values.

V. Discussions

The GLASS LAI retrieval algorithm uses GRNNs to retrieve LAI values from time-series MODIS/AVHRR reflectance data. Training with representative samples is of critical importance in any neural-network-based retrieval algorithm. Instead of simulated data, the GRNNs were trained using fused time-series LAI values from MOD15 and CYCLOPES LAI products and preprocessed MODIS/AVHRR reflectance data over the BELMANIP sites. Several global LAI products were retrieved from satellite observations based on existing LAI products. The GEOV1 LAI retrieval algorithm relies on back-propagation neural networks trained with the "best estimates" of LAI obtained by fusing and scaling the MOD15 and CYCLOPES LAI products and the SPOT/VEGETATION nadir surface reflectance values over the BELMANIP sites [24]. The GIMMS3g LAI retrieval algorithm relies on feedforward neural

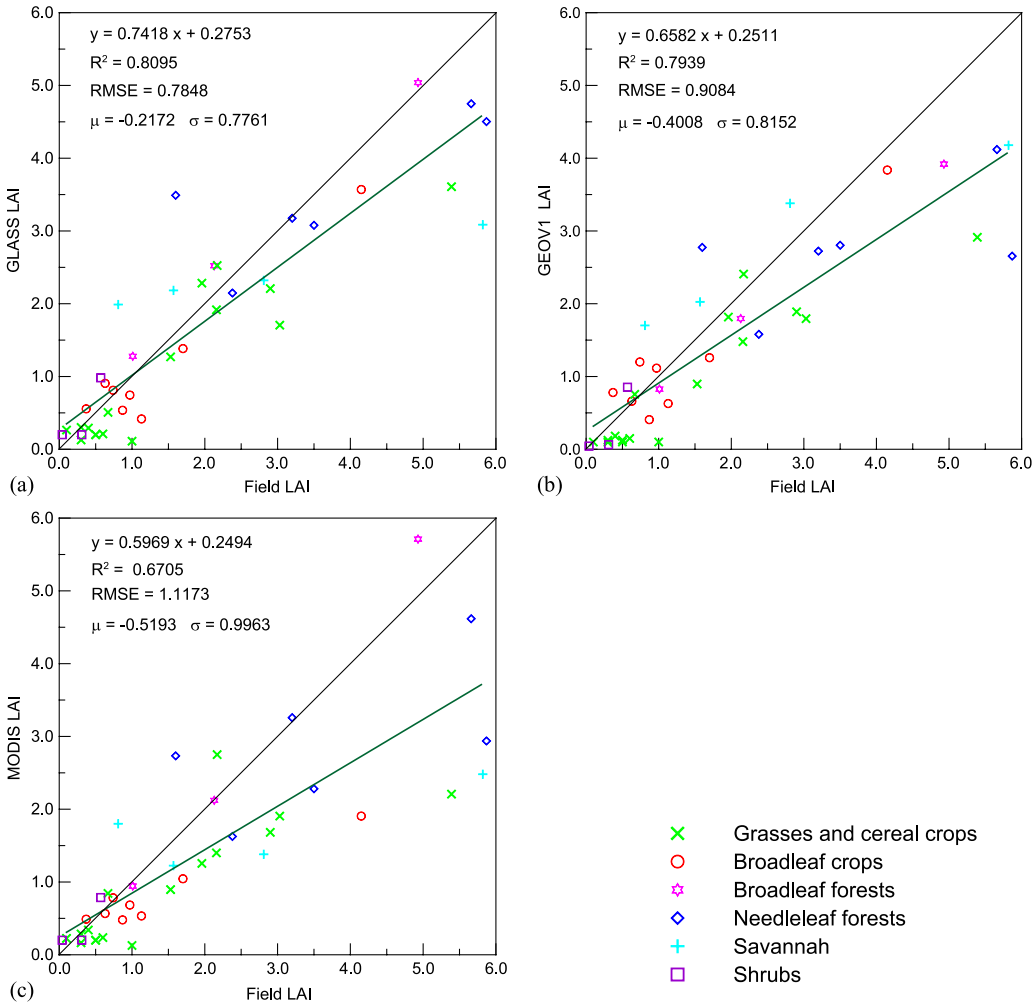

Fig. 13. Scatterplots of (a) GLASS, (b) GEOV1, and (c) MOD15 LAI values versus mean values of high-resolution LAI maps for direct validation. The regression function, R^2, RMSE, μ, and σ are also shown.

networks trained with the best-quality MOD15 LAI product and GIMMS3g NDVI data [23].

A unique feature of the GLASS LAI retrieval algorithm is that the LAI annual profile is estimated using annual observations. Unlike existing neural network methods that use remote sensing data acquired only at a specific time to retrieve LAI, the GRNNs used in GLASS LAI production use the surface reflectance for a one-year period as their input, and their output is the one-year LAI profile for each pixel. Therefore, the retrieval algorithm can remove abrupt spikes and dips and generate temporally continuous and smooth LAI profiles. The long time series of the GLASS LAI product is very suitable for long-term research in fields such as agricultural sustainability, forest ecosystems, and global changes.

Nevertheless, the surface-reflectance data for a one-year period were entered into the GRNNs to estimate the one-year LAI profiles. Therefore, the GLASS LAI retrieval algorithm is essentially a reanalysis method. It is impossible to provide near-real-time retrievals from satellite observations. This is one of the weaknesses of the GLASS LAI retrieval algorithm compared with the MOD15 and GEOV1 LAI retrieval algorithms, which can generate LAI products from remotely sensed data in near real time for hazard/disaster monitoring and warning. In addition, the GLASS LAI retrieval algorithm can also remove abrupt spikes and dips, which may lead to the loss of neighboring smaller peaks in LAI profiles. For example, in Fig. 10(a), the GLASS LAI profile over the Sud-Ouest site does not reproduce the expected double peak during the growing seasons in 2002 and 2003.

VI. Conclusion

A method previously proposed has been improved to generate the GLASS LAI product for 1981–2014 from MODIS and AVHRR reflectance time-series data. The consistency of GLASS LAI values derived from AVHRR and MODIS reflectance data was evaluated, and the quality and accuracy of the GLASS LAI product were assessed in this study through comparisons with MOD15 and GEOV1 LAI products and direct comparisons with high-resolution LAI maps.

The results have demonstrated that the GLASS LAI values derived from MODIS and AVHRR reflectance data form a consistent data set at a spatial resolution of 0.05°. Comparisons of the GLASS LAI product with the MOD15 and GEOV1 LAI products indicated that these LAI products are generally consistent in their spatial patterns. The global consistency of

these LAI products is good in most situations, particularly for grasses/cereal crops and shrubs. However, a relatively large discrepancy among these LAI products was observed in tropical forest regions, where GEOV1 LAI values were clearly lower than the GLASS and MOD15 LAI values, particularly in January. Temporal consistency analysis showed that the temporal profiles of all these LAI products exhibited consistent seasonal variations. The GLASS and GEOV1 LAI products provided smooth trajectories, whereas the MOD15 LAI product showed less stable profiles, particularly during growing seasons. Quantitative comparison of these temporal profiles demonstrated that the temporal smoothness of the GLASS LAI product was superior to that of the GEOV1 and MODIS LAI products.

Direct validation with mean values of high-resolution LAI maps showed that the GLASS LAI values were closer to the mean values of these maps than the GEOV1 and MODIS LAI values. All these LAI products showed better performance for low LAI values than for high LAI values, but the GLASS LAI values were in better agreement with the mean values of the high-resolution LAI maps than the GEOV1 and MOD15 LAI values, particularly for higher LAI values.

The validation of LAI products, however, is limited by LAI ground measurements, most of which have been available since 2000. In the near future, the authors hope to carry out more extensive validation and analysis of the GLASS LAI values derived from AVHRR reflectance data by searching for ground measurements for direct validation and by integrating key climate variables such as temperature and precipitation for indirect validation.

ACKNOWLEDGMENT

The GLASS LAI product is generated and released by the Center for Global Change Data Processing and Analysis of Beijing Normal University (http://www.bnu-datacenter.com/). It can also be downloaded from the University of Maryland Global Land Cover Facility (http://glcf.umd.edu). The authors would like to thank LTDR for providing AVHRR data, particularly Dr. E. Vermote for his valuable assistance, and the anonymous reviewers for their constructive comments that greatly helped improve the quality of this paper.

REFERENCES

[1] I. Jonckheere *et al.*, "Review of methods for *in situ* leaf area index determination Part I. Theories, sensors and hemispherical photography," *Agricultural Forest Meteorol.*, vol. 121, pp. 19–35, 2004.

[2] L. He, J. M. Chen, J. Pisek, C. B. Schaaf, and A. H. Strahler, "Global clumping index map derived from the MODIS BRDF product," *Remote Sens. Environ.*, vol. 119, pp. 118–130, 2012.

[3] S. Liang, "Recent developments in estimating land surface biogeophysical variables from optical remote sensing," *Progress Phys. Geogr.*, vol. 31, no. 5, pp. 501–516, 2007.

[4] H. Fang, Z. Xiao, Y. Qu, and J. Song, *Leaf Area Index in Advanced Remote Sensing: Terrestrial Information Extraction and Applications*, S. Liang, X. Li, and J. Wang, Eds. Oxford, U.K.: Academic, 2013, Ch. 11, pp. 317–348.

[5] F. Wang, J. Huang, Y. Tang, and X. Wang, "New vegetation index and its application in estimating leaf area index of rice," *Rice Sci.*, vol. 14, no. 3, pp. 195–203, 2007.

[6] F. Gascon, J. P. Gastellu-Etchegorry, M. J. Lefevre-Fonollosa, and E. Dufrene, "Retrieval of forest biophysical variables by inverting a 3-D radiative transfer model and using high and very high resolution imagery," *Int. J. Remote Sens.*, vol. 25, no. 4, pp. 5601–5616, 2004.

[7] Z. Xiao, S. Liang, J. Wang, J. Song, and X. Wu, "A temporally integrated inversion method for estimating leaf area index from MODIS data," *IEEE Trans. Geosci. Remote Sens.*, vol. 47, no. 8, pp. 2536–2545, Aug. 2009.

[8] R. B. Myneni *et al.*, "Global products of vegetation leaf area and fraction absorbed PAR from year one of MODIS data," *Remote Sens. Environ.*, vol. 83, pp. 214–231, 2002.

[9] F. Baret *et al.*, "LAI, fAPAR and fCover CYCLOPES global products derived from VEGETATION. Part 1: Principles of the algorithm," *Remote Sens. Environ.*, vol. 110, pp. 275–286, 2007.

[10] Y. Liu, R. Liu, and J. M. Chen, "Retrospective retrieval of long-term consistent global leaf area index (1981–2011) from combined AVHRR and MODIS data," *J. Geophys. Res.—Biogeosci.*, vol. 117, 2012, Art. no. G04003.

[11] S. Ganguly *et al.*, "Generating vegetation leaf area index earth system data record from multiple sensors. Part 1: Theory," *Remote Sens. Environ.*, vol. 112, no. 12, pp. 4333–4343, 2008.

[12] F. Camacho, J. Cernicharo, R. Lacaze, F. Baret, and M. Weiss, "GEOV1: LAI, FAPAR essential climate variables and FCOVER global time series capitalizing over existing products. Part 2: Validation and intercomparison with reference products," *Remote Sens. Environ.*, vol. 137, pp. 310–329, 2013.

[13] S. Garrigues *et al.*, "Validation and intercomparison of global Leaf Area Index products derived from remote sensing data," *J. Geophys. Res.*, vol. 113, 2008, Art. no. G02028.

[14] W. Yang *et al.*, "MODIS leaf area index products: From validation to algorithm improvement," *IEEE Trans. Geosci. Remote Sens.*, vol. 44, no. 7, pp. 1885–1898, Jul. 2006.

[15] M. Weiss, F. Baret, S. Garrigues, and R. Lacaze, "LAI, fAPAR and fCover CYCLOPES global products derived from VEGETATION. Part 2: Validation and comparison with MODIS collection 4 products," *Remote Sens. Environ.*, vol. 110, no. 3, pp. 317–331, 2007.

[16] H. Fang, S. Liang, J. Townshend, and R. Dickinson, "Spatially and temporally continuous LAI data sets based on an integrated filtering method: Examples from North America," *Remote Sens. Environ.*, vol. 112, pp. 75–93, 2008.

[17] R. Fensholt, I. Sandholt, and M. S. Rasmussen, "Evaluation of MODIS LAI, fAPAR and the relation between fAPAR and NDVI in a semi-arid environment using *in situ* measurements," *Remote Sens. Environ.*, vol. 91, no. 3/4, pp. 490–507, 2004.

[18] J. Pisek and J. M. Chen, "Comparison and validation of MODIS and VEGETATION global LAI products over four BigFoot sites in North America," *Remote Sens. Environ.*, vol. 109, no. 1, pp. 81–94, 2007.

[19] Q. Liu *et al.*, "Assimilation of satellite reflectance data into a dynamical leaf model to infer seasonally varying leaf areas for climate and carbon models," *J. Geophys. Res.*, vol. 113, 2008, Art. no. D19113.

[20] Z. Xiao, S. Liang, J. Wang, B. Jiang, and X. Li, "Real-time retrieval of Leaf Area Index from MODIS time series data," *Remote Sens. Environ.*, vol. 115, no. 1, pp. 97–106, 2011.

[21] F. Deng, J. M. Chen, S. Plummer, M. Chen, and J. Pisek, "Global LAI algorithm integrating the bidirectional information," *IEEE Trans. Geosci. Remote Sens.*, vol. 44, no. 8, pp. 2219–2229, Aug. 2006.

[22] Y. Knyazikhin, J. V. Martonchik, R. B. Myneni, D. J. Diner, and S. W. Running, "Synergistic algorithm for estimating vegetation canopy leaf area index and fraction of absorbed photosynthetically active radiation from MODIS and MISR data," *J. Geophys. Res.*, vol. 103, pp. 32 257–32 275, 1998.

[23] Z. Zhu *et al.*, "Global data sets of vegetation leaf area index (LAI)3g and fraction of photosynthetically active radiation (FPAR)3g derived from global inventory modeling and mapping studies (GIMMS) normalized difference vegetation index (NDVI3g) for the period 1981 to 2011," *Remote Sens.*, vol. 5, pp. 927–948, 2013.

[24] F. Baret *et al.*, "GEOV1: LAI and FAPAR essential climate variables and FCOVER global time series capitalizing over existing products. Part 1: Principles of development and production," *Remote Sens. Environ.*, vol. 137, pp. 209–309, 2013.

[25] S. Liang *et al.*, "A long-term global land surface satellite (GLASS) dataset for environmental studies," *Int. J. Digital Earth*, vol. 6, pp. 5–33, 2013.

[26] A. Verger, F. Baret, and M. Weiss, "A multisensor fusion approach to improve LAI time series," *Remote Sens. Environ.*, vol. 115, no. 10, pp. 2460–2470, 2011.

[27] Z. Xiao *et al.*, "Use of general regression neural networks for generating the GLASS leaf area index product from time series MODIS surface reflectance," *IEEE Trans. Geosci. Remote Sens.*, vol. 52, no. 1, pp. 209–223, Jan. 2014.

[28] E. F. Vermote and A. Vermeulen, "Atmospheric correction algorithm: Spectral reflectances (MOD09)," Nat. Aeronaut. Space Admin. (NASA), Washington, DC, USA, Algorithm Theoret. Background Doc., 1999. [Online]. Available: http://modarch.gsfc.nasa.gov/MODIS/ATBD/atbd_mod08.pdf
[29] J. Pedelty *et al.*, "Generating a long-term land data record from the AVHRR and MODIS instruments," *Proc. IEEE Int. Geosci. Remote Sens. Symp.*, 2007, pp. 1021–1025.
[30] H. Tang *et al.*, "A cloud detection method based on a time series of MODIS surface reflectance images," *Int. J. Digital Earth*, vol. 6, pp. 157–171, 2013.
[31] B. N. Holben, "Characteristics of maximum-value composite images for temporal AVHRR data," *Int. J. Remote Sens.*, vol. 7, pp. 1435–1445, 1986.
[32] "GCTP general cartographic transformation package software documentation," U.S. Dept. Interior, U.S. Geological Survey, Nat. Mapping Div. 1993.
[33] J. M. Welles and J. M. Norman, "Instrument for indirect measurement of canopy architecture," *Agronomy J.*, vol. 83, no. 5, pp. 818–825, 1991.
[34] J. M. Chen and J. Cihlar, "Plant canopy gap-size analysis theory for improving optical measurements of leaf-area index," *Appl. Opt.*, vol. 34, pp. 6211–6222, 1995.
[35] V. Demarez, S. Duthoit, M. Weiss, F. Baret, and G. Dedieu, "Estimation of leaf area index (LAI) of wheat, maize and sunflower crops using digital hemispherical photographs," *Agricultural Forest Meteorol.*, vol. 148, no. 4, pp. 644–655, 2008.
[36] J. Morisette *et al.*, "Validation of global moderate resolution LAI products: A framework proposed within the CEOS land product validation subgroup," *IEEE Trans. Geosci. Remote Sens.*, vol. 44, no. 7, pp. 1804–1817, Jul. 2006.
[37] W. B. Cohen *et al.*. "MODIS land cover and LAI collection 4 product quality across nine sites in the western hemisphere," *IEEE Trans. Geosci. Remote Sens.*, vol. 44, no. 7, pp. 1843–1858, Jul. 2006.
[38] M. Weiss, "Valeri 2003: Barrax site (Cropland). Ground data processing & production of the level 1 high resolution maps," INRA-CSE, Avignon, France, 2004. [Online]. Available: http://www.avignon.inra.fr/valeri
[39] R. A. Fernandes, C. Butson, S. Leblanc, and R. Latifovic, "Landsat-5 TM and Landsat-7ETM+ based accuracy assessment of leaf area index products for Canada derived from SPOT4/VGT data," *Can. J. Remote Sens.*, vol. 29, no. 2, pp. 241–258, 2003.
[40] A. Cescatti *et al.*, "Intercomparison of MODIS albedo retrievals and *in situ* measurements across the global FLUXNET network," *Remote Sens. Environ.*, vol. 121, pp. 323–334, Jun. 2012.
[41] J. Pisek, J. Chen, R. Lacaze, O. Sonnentag, and K. Alikas, "Expanding global mapping of the foliage clumping index with multi-angular POLDER three measurements: Evaluation and topographic compensation," *ISPRS J. Photogramm. Remote Sens.*, vol. 65, pp. 341–346, 2010.
[42] D. F. Specht, "A general regression neural network," *IEEE Trans. Neural Netw.*, vol. 2, no. 6, pp. 568–576, Nov. 1991.
[43] H. Fang *et al.*, "Characterization and intercomparison of global moderate resolution leaf area index (LAI) products: Analysis of climatologies and theoretical uncertainties," *J. Geophys. Res.—Biogeosci.*, vol. 118, pp. 529–548, 2013.
[44] N. V. Shabanov *et al.* "Analysis and optimization of the MODIS leaf area index algorithm retrievals over broadleaf forests," *IEEE Trans. Geosci. Remote Sens.*, vol. 43, no. 8, pp. 1855–1865, Aug. 2005.
[45] W. B. Cohen *et al.*, "Comparisons of land cover and LAI estimates derived from ETM+ and MODIS for four sites in North America: A quality assessment of 2000/2001 provisional MODIS products," *Remote Sens. Environ.*, vol. 88, pp. 233–255, 2003.

Zhiqiang Xiao received the Ph.D. degree in geophysical prospecting and information technology from Central South University, Changsha, China, in 2004.

From 2004 to 2006, he was a Postdoctoral Research Associate with Beijing Normal University, Beijing, China. His research focuses on the retrieval of land biophysical parameters from remotely sensed data, assimilating radiometric observations into dynamic models.

Shunlin Liang (M'94–F'13) received the Ph.D. degree from Boston University, Boston, MA, USA.

He is currently a Professor with the Department of Geographical Sciences, University of Maryland, College Park, MD, USA, and the School of Geography, Beijing Normal University, Beijing, China. He has published approximately 260 SCI-indexed journal papers, authored the book *Quantitative Remote Sensing of Land Surfaces* (Wiley, 2004), coauthored the book *Global LAnd Surface Satellite (GLASS) Products: Algorithms, Validation and Analysis* (Springer, 2013), edited the book *Advances in Land Remote Sensing: System, Modeling, Inversion and Application* (Springer, 2008), and coedited the books *Advanced Remote Sensing: Terrestrial Information Extraction and Applications* (Academic Press, 2012) and *Land Surface Observation, Modeling, Data Assimilation* (World Scientific, 2013). His main research interests focus on the estimation of land surface variables from satellite data, earth energy balance, and assessment of environmental changes.

Dr. Liang was an Associate Editor of the IEEE TRANSACTIONS ON GEOSCIENCE AND REMOTE SENSING and a Guest Editor of several remote-sensing-related journals.

Jindi Wang received the B.S. degree from the Beijing University of Posts and Telecommunications, Beijing, China, in 1982.

She is currently a Professor with the State Key Laboratory of Remote Sensing Science, Research Center for Remote Sensing and Geographic Information Systems, Beijing Normal University, Beijing. Her primary research interests focus on land surface bidirectional reflectance distribution function modeling, land surface parameter retrieval, and typical land surface objects' spectrum library building and its application.

Yang Xiang received the B.S. degree in geography information systems from Wuhan University, Wuhan, China, in 2011 and the M.S. degree in remote sensing and geographic information systems from Beijing Normal University, Beijing, China, in 2014.

Her current research is focused on the retrieval of biophysical variables from remote sensing data.

Xiang Zhao received the Ph.D. degree in cartography and geographic information systems from Beijing Normal University, Beijing, China, in 2006.

During 2008–2010, he was a Postdoctoral Fellow with the College of Resources Science and Technology, Beijing Normal University. His main research interests focus on high-performance computing system construction and quantitative remote sensing application. He also did some research on long-time-series remote sensing data trend analysis.

Jinling Song received the Ph.D. degree in remote sensing and geographic information systems from Beijing Normal University, Beijing, China, in 2006.

From 2006 to 2008, she was a Postdoctoral Research Associate with Beijing Normal University. Her research is directed toward computer simulation and parameter retrieval of vegetation.